AIMS Materials Science, 11(4): 712–759.
DOI: 10.3934/matersci.2024036
Received: 20 June 2024
Revised: 30 July 2024
Accepted: 13 August 2024
Published: 27 August 2024

http://www.aimspress.com/journal/Materials

Review

Sustainable $A_2B^IB^{III}X_6$ based lead free perovskite solar cells: The challenges and research roadmap for power conversion efficiency improvement

Etsana Kiros Ashebir, Berhe Tadese Abay and Taame Abraha Berhe*

Department of Chemistry, Adigrat University, Adigrat, 50, Ethiopia

* **Correspondence:** Email: taame.abraha@adu.edu.et; taameabr188@gmail.com; Tel: +251-983-159-245.

Abstract: The stability issues in the widely known $CH_3NH_3PbI_3$, lead to the development of alternative halide double perovskite materials, which has received great attention in recent times. Although the stability issue of double halide perovskite seems promising, their device performance remains far inferior to $CH_3NH_3PbI_3$ and with challenges for further improvements. Furthermore, the power conversion efficiency of single junction organic-inorganic halide perovskite is now 24.2% and 29.15% for the textured monolithic perovskite/silicon tandem solar cell; however, for the all-inorganic halide perovskite solar cell, it is 7.11%, and halide double perovskite solar cells are based on $A_2B^IB^{III}X_6$ (A = monocation, B = cation or vacancy, X = halide) such as $Cs_2AgBiBr_6$, Cs_2TiBr_6, $Cs_2AgTlBr_6$ and $Cs_2Ag(Bi_{1-x}In_x)Br_6$, being 2.8% and 3.3%, respectively. This creates big questions and concerns about the performance improvement of $A_2B^IB^{III}X_6$-based perovskite solar cells. Not only is this a concern, but there are many other big challenges faced by halide double perovskite solar cells. Such big challenges include: (a) geometric constraints and limited integration with interfacial materials; (b) dynamic disorder, a wide band gap, and a localized conduction band caused by a cubic unit cell that restrains the interactions of orbitals; (c) high processing temperature which may limit the diverse applications; and (d) low electronic dimensionality that makes them less appropriate for single junction solar cell purpose, etc. Moreover, the origin of electronic and optical properties such as the polarizability, the presence of molecular dipoles, and their influence on the

dynamics of the photo-excitations remain bottleneck concerns that need to be elucidated. We roadmap performance sustainable improvement, which is suggested with a particular focus on engineering material surface and bulk, band gap, interfacial, composition, doping, device architectural, polar, and domain order. The reason that this review was developed was to forward great contributions to the readers and commercial ventures.

Keywords: sustainability; $Cs_2AgBiBr_6$; Cs_2TiBr_6; all inorganic; halide double perovskite

1. Introduction

A definitive objective of materials utilized in optoelectronic applications ought to be founded on the "triple-E" terms: financially economical, vitality effective, and naturally efficient. Despite their very great execution in lead halide perovskite based solar cells with efficiencies reaching 24.2% and the rising application for lasers [1], light-radiating diodes (LEDs) [2], field-impact light-producing transistors (FETs) [3], organic−inorganic lead halide perovskites experience the ill effects of substances of lethal, contaminating, and bioaccumulative Pb, which may, in the end, hamper their commercialization. Progressively, it turns out to be of essential significance to consider and create alternative classes of lead-free halide double perovskites for various optoelectronic applications [4].

The need to create practical advances is dependent on ecologically neighborly, earth-inexhaustible, and financially savvy materials that normally drive the consideration toward the change metals with especially appealing metals (e.g., Fe^{2+}, Cu^{2+}, Zn^{2+}) and post-transition elements [5,6]. For example, tin [7,8], rubidium [9,10], indium-silver [11,12], titanium [13], bismuth and silver-bismuth [11,14–17], and copper [18] based perovskites have been found as potential choices to toxic perovskites. Thanks to their rich science, their utilization may tremendously broaden engineered courses of new halide double perovskites for photovoltaic and light-radiating applications, enhancing the tunability of the material. Moreover, the discovery of lead-free double perovskites provides a feasible way of searching for air-stable and environmentally benign solar cell absorbers [19–23]. Since the 1970s, a large number of double perovskites (which are well known as elpasolites) with nominal chemical compositions of $A_2B^IB^{III}X_6$ (A and B^I = Li^+, Na^+, K^+, Rb^+, Cs^+, Ag^+, Tl^+, etc., B^{III} = Bi^{3+}, Al^{3+}, Ln^{3+}, Ga^{3+}, Fe^{3+}, etc., and X = F, Cl, Br, or I) have been initially reported as ferroelectric materials [24,25]. However, the lead and tin free all-inorganic halide double perovskite solar cell power conversion efficiency is far smaller than the power conversion efficiency (PCE) of lead based perovskite solar cells. The lead and tin free all-inorganic halide double perovskites PCE improvement is too slow compared to lead halide perovskites PCE, which has become a great concern and active research direction for the halide double perovskite scientific community. In conjunction with the advancement of halide double perovskite solar cells, interesting concepts covering cationic exchange, doping, and alloying for engineering the electronic structure of double perovskites [26], its crystal structure include preparation approaches, physicochemical properties, and material applications [6,27,28] with various strategies such as hetero-substitution of Pb to form quaternary halide double perovskites [5] and a strategy for achieving small band gaps in this family of materials [29]. Moreover, the PCE of

single junction lead based perovskite is now 24.2% [30], 25.2% [31], and 29.15% [32] for the textured monolithic perovskite/silicon tandem solar cell, but the record for lead-free all inorganic cesium tin-germanium triiodide ($CsSn_{0.5}Ge_{0.5}I_3$) solid-solution perovskite is 7.11% [33]. According to the simulation results reported, $CsSn_{0.5}Ge0.5I_3$ perovskite material can have a power conversion efficiency of 18.79% [34] and 24.63% [35]. Furthermore, the $CsSn_{0.5}Ge_{0.5}I_3/FASnI_3$ device architecture is reported with a simulated power conversion efficiency of 31.58% [36]. This indicates that the $CsSn_{0.5}Ge_{0.5}I_3/FASnI_3$ device is a promising device for high-performance lead-free solar cells.

This efficiency can be achieved if encapsulation mechanisms, fabrication procedures, and material parameters such as defect density, layer thickness, operating temperature, electron affinity, and potential energy are well optimized during an experiment. Moreover, tin-based perovskite solar cells have promising efficiency next to lead-based perovskite solar cells as devices made of Tin based perovskite materials exhibit insufficient stability [37] and contain intrinsically deep defects that are detrimental to the perovskite solar cell performance [38]. Even the most stable $CsSn_{0.5}Ge_{0.5}I_3$ based perovskite solar cell showed 10% decay efficiency after 500 h of continuous operation in an N_2 atmosphere under one-sun illumination [33]. Hence, to overcome the toxicity of lead and insufficient stability of Tin, efforts to find alternative perovskite materials, which are earth-abundant, non-toxic, stable, and biocompatible, are in progress.

Based on these needs, lead and tin free $A_2B^IB^{III}X_6$ based all-inorganic solar cells such as $Cs_2AgBiBr_6$ and Cs_2TiBr_6 have been reported recently [39]. The records for $Cs_2AgBiBr_6$ and Cs_2TiBr_6 lead and a tin-free, all-inorganic halide double perovskite solar cell are 2.5% [40] (current report is 2.81% [41] with a photoelectronic conversion efficiency of hydrogenated $Cs_2AgBiBr_6$ perovskite solar cell of 6.37% [42]) and 3.3% [43], respectively. These are far less than 24.2% for single junction lead-based halide perovskite solar cells and 29.15% for a tandem solar cell. Consequently, the progress is too slow to reach the hybrid lead halide perovskite solar cells. From a theoretical perspective, simulation results reported that Cs_2TiBr_6 has achieved 11.49% power conversion efficiency [44]. This is promising for manufacturing practical lead-free, double halide perovskite solar cells. More recently, an $Au/CuSbS_2/Cs_2TiBr_6/CdS/TCO$ configuration has achieved a power conversion efficiency of 23.77%, as reported by simulated results [45]. This is again a more promising result in this field. Unless the real and bottleneck challenges and solutions are clearly identified, the $Cs_2AgBiBr_6$ and Cs_2TiBr_6 based halide double perovskite solar cell will not be the first alternative solar cell to replace the hybrid lead halide perovskite solar cells. Thus, this review article is designed to identify the challenges and possible solutions for power conversion efficiency improvement of halide, double perovskite solar cells that will be considered a research roadmap for performance improvements in this field. Hence, this is a comprehensive review that concisely reviews the modification strategies from $CH_3NH_3PbI_3$ into many halide double perovskite materials, the origin of electronic and optical properties variations, and key challenges and areas of research for possible solutions and performance improvement strategies of both Lead and Tin free all-inorganic halide double perovskite solar cells. Moreover, this will provide a new perspective and research roadmap for performance improvement to the scientific community and research industries.

2. Issue of sustainability in lead-based halide perovskite solar cells

The issue of sustainability in lead halide perovskite solar cells is the biggest challenge. This sustainability concept is not only understood in terms of economic viability, toxicity, and stability but also affordability, availability of materials, energy independence, quality of being able to continue over a period of time, free of hazardous materials, etc. Now, we question whether $A_2B^IB^{III}X_6$ such as $Cs_2AgBiBr_6$ and Cs_2TiBr_6 based perovskite solar cells can answer all concepts of sustainability so that it can revolutionize the photovoltaic field of research or not? We seek to answer this question.

3. Promising candidate properties to substitute Pb metal

The organic-inorganic halide perovskites become capable of photovoltaic and energy applications beyond photovoltaic. However, the large scale commercialization of the perovskite harvester faces considerable limitations due to the toxicity of lead metal and the perovskite absorber degradation [6,46–48]. For this reason, there is an interest to discover nontoxic and stable perovskites for the betterment of this field. The degradation concern can be treated by carbon encapsulation, multi-cation substitution, and incorporation of hydrophobic moieties [47,49]. On the other hand, substitution of Pb using non-toxic transition metal atoms is the single strategy to overcome the toxicity problems [46,50,51]. Consequently, the optoelectronic properties [52] such as direct band gaps [19,53], electron mobility [54], defect tolerance, high absorption coefficient [55], small carrier effective masses, intrinsic thermodynamic stability [56], long charge carrier diffusion lengths [57], low exciton binding energies, higher dielectric constant, and compatibility with low-cost and solution-supported fabrication procedures [58] are considered promising candidate properties to replace lead-based solar cell light harvesting materials in perovskite solar cells. Solving the predictable restrictions of solution-processed semiconductors is another important candidate topic that needs to be considered in the lead replacement process [59–63]. Moreover, there are promising candidate materials that can overcome the issue of toxicity, instability, lifetime, and device deterioration of lead based halide perovskite. Such materials are the topic of this review, with a general formula assigned as $A_2B^IB^{III}X_6$ based lead free perovskite solar cells.

4. Modification strategies from $CH_3NH_3PbI_3$ into $Cs_2AgBiBr_6$ and Cs_2TiBr_6 halide double perovskites

Solar cell devices made of organic-inorganic lead halide perovskite material ($CH_3NH_3PbI_3$) has been reported in 2009 with a cell efficiency of 3.81% [64], indicating that $CH_3NH_3PbI_3$ with an efficiency of 24.2% [30] was achieved in 2019 and has reached 29.15% [32]. This is promising if the device made further optimized continuously. Gradually, modification of $CH_3NH_3PbI_3$ has been done at three sites, as shown in Scheme 1 [65]: strategy (1) halogen atoms like chlorine, bromine, and a combination of all these halogens [66–69]; strategy (2) organic part [70–73]; and strategy (3) at an inorganic Pb metal site such as Ge [74], resulting in many derivatives of $CH_3NH_3PbI_3$ materials classified as organic-inorganic perovskites, fully inorganic perovskites, and halide double

perovskites etc. All these modifications are the subject of this section and are classified as cation displacement at A and B site and anion displacement at X-site. Furthermore, all these cation and anion modifications, as well as the tunable structural dimensions, cation-anion order-disorder, distortions, and tilting of the octahedral unit, BX_6, from the ideal structure, are collectively considered as the origin of diversity in materials structure, dimension, and optoelectronic properties. Based on these modifications, iodide, bromide, mixed metals, and mixed I/Br ratio-based double perovskites such as $Cs_2AgBiBr_6$, $Cs_2AgBiCl_6$, $Cs_2AgInCl_6$, $Cs_2NaBiCl_6$, $Cs_2Ag(Sb_xBi_{1-x})Br_6$, and $Cs_2AgBi(Br/I)_6$ or $Cs_2AgBiBr_{6-x}I_x$, have become widely known double perovskite light absorbing materials [75]. The challenge in these materials is the large band gap. To solve this challenge, compositional engineering plays a great role in discovering new optical and electrical properties in these materials. Mixed compositions in the metal and halogen site have been investigated to explore these materials [76,77]. This approach helps to discover stable and nontoxic halide double perovskite materials, which are the main focus of this review.

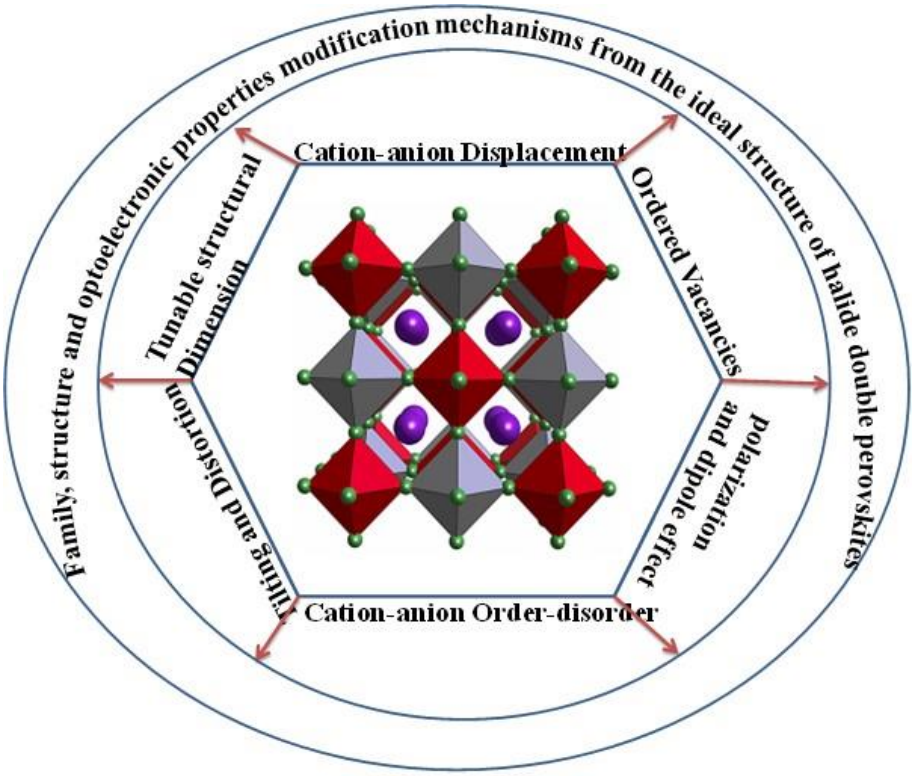

Scheme 1. Halide double perovskite family, structure, and optoelectric property modification mechanisms.

5. Origin of electronic and optical property variations

In addition to the structural variations, optoelectronic properties such as absorption, electron-hole diffusion length, carrier life time, carrier mobility, charge carrier dynamics, electronic structure such as band structure and density of state, effective mass of electron, thermal properties, and other electrical properties such as ferroelectric, pyroelectric, and piezoelectric properties are the

major material properties that cause differences in device efficiency; moreover, everyone wants to deal with this for further energy application of materials [78]. Recently, the field of organic-inorganic hybrid halide perovskite has revolutionized the field of photovoltaics. Moreover, modifying the halide perovskites gives new halide double perovskites for which the stated properties are not well studied. Thus, understanding the origin of these optoelectronic property variations would be of great interest for the development of halide double perovskite material performance. In this section, molecular dipoles, tilting of octahedron, transition metal cation size and its oxidation states, band structure, photoluminescence, and other optoelectric properties are considered as potential origins of improvement of the performance for $Cs_2AgBiBr_6$ and Cs_2TiBr_6 halide double perovskite solar cells.

5.1. Effect of polarization and molecular dipoles on the dynamics of photo-excitations

Regardless of fast improvements in both photovoltaic and light producing device execution, the comprehension of the optoelectronic properties of halide double perovskites is as yet fragmented. Specifically, the polarization of the material, the nearness of sub-atomic dipoles, and their impact on the dynamics of the photo-excitations remains an open issue to be cleared up. From now on, the imperative subject of discussion has been the seemingly perpetual polarization of the perovskite under connected electric fields [79,80]. This impact shows itself as a huge hysteresis in the deliberate current–voltage curve of perovskite sun-oriented cells and LEDs in planar hetero-junction designs, contingent upon the contact materials used [79,81,82]. The vast majority of the ongoing work underpins the speculation that particle migration [79,82,83] ought to rule any ferroelectric conduct at room temperature [84]. In addition to these polarization effects, there is another effect that causes problems in efficiency estimation [85]. The hysteresis effect transforms the dominant behavior from normal (Figure 1a−c) to be inverted (Figure 1d−f) owing to the decreasing scan rate with a stabilized current−voltage curve at an equilibrium point [86]. The estimated efficiency in the inverted behavior is different from the dominant normal behavior. Those devices showing high efficiency have lower surface recombination that can be a source of the hysteresis effect. Moreover, the presence of the hysteresis effect originates from ion migration, charge carrier trapping/detrapping, and ferroelectric polarization [87]. This hysteresis effect is not only affecting device efficiency but also device stability [87]. Owing to its negative impact on efficiency and stability, mechanisms to avoid its presence via strategies such as either working on device architecture, increasing grain sizes, interface engineering, and additive doping have been suggested [87,88].

Researchers such as Leijtens et al. [89] explored the impact of a connected outer electric field on the photograph-energized types of $CH_3NH_3PbI_3$ thin movies, both at room temperature and at low temperature, by checking the photoluminescence (PL) yield and PL rots. At room temperature, these creators discovered proof for an electric field–incited decrease of radiative bimolecular bearer recombination together with the movement of charged imperfections that influence the non-radiative rot rate of the photoexcited species. This has been allotted to field-incited arrangement of the atomic dipoles, which diminishes the vibrational opportunity of the cross section and the related nearby screening, which results in a more grounded electron gap interaction [89].

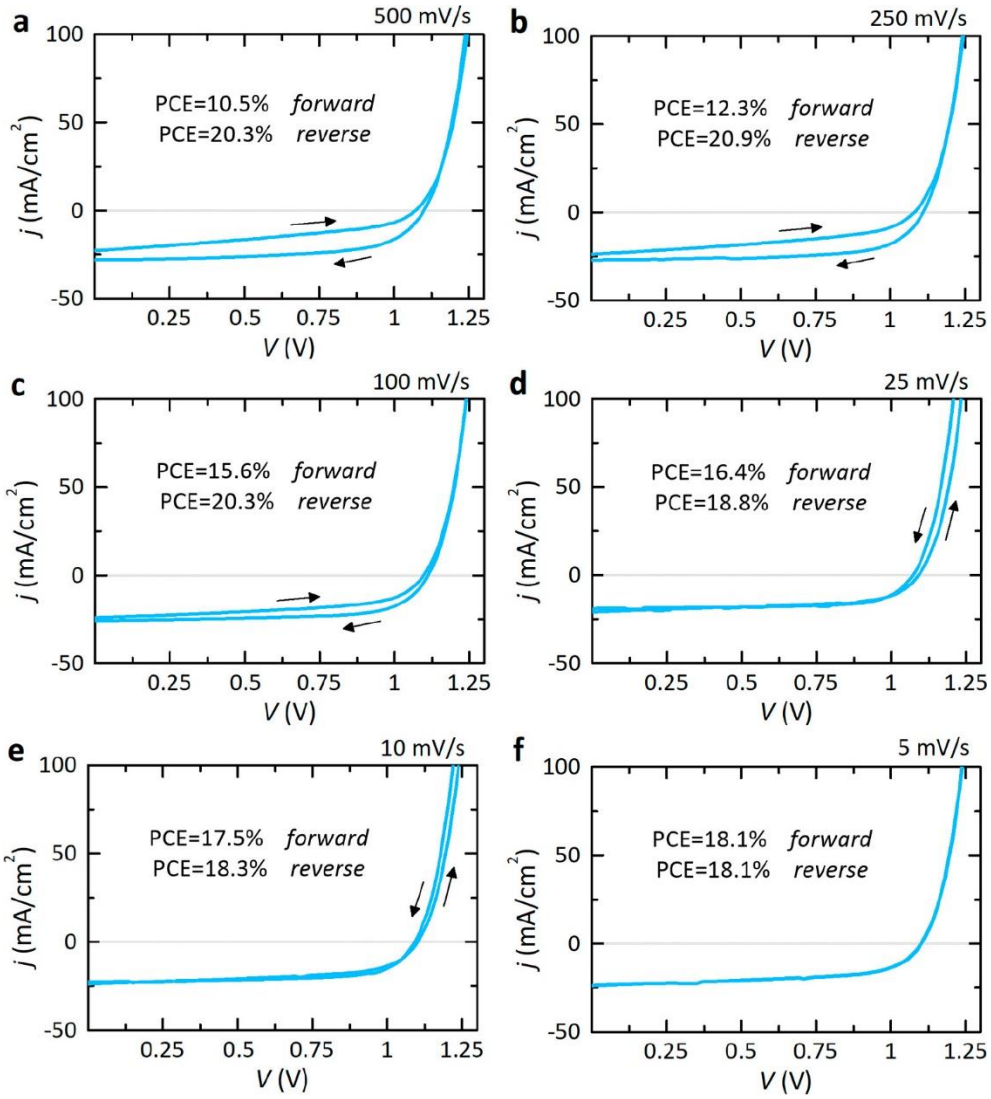

Figure 1. Hysteresis tracing current–voltage curves at different voltage sweep rates of (a) 500, (b) 250, (c) 100, (d) 25, (e) 10, and (f) 5 mV/s (Reproduced from Ref. [86] with permission).

5.2. Effects of tilting on the band structure and electron-hole transport

Diverse degrees of tilting of the octahedral structure offer ascent to various precious crystal fields, which results in various electronic and optical properties. The degrees of tilting may influence the band structure, electron transport properties, photoluminescence, and dielectric conduct. Tilting at the organic cage causes distortion of peroveskite lattice either by tilting at PbX_6 octahedra or brings isotropic lattice contractions. In the first case, it increases the band gap by reducing orbital overlap; in the second case, it reduces the band gap [90–92]. Understanding characteristics of inorganic octahedral tilt is an important issue to understand band structure and electron hole transport in halide perovskite materials. In this case, corner connected octahedral structure where distortion, including octahedral tilting, plays its own role. This lattice distortion brings structural flexibility where various phases are created; not only octahedral tilting but also off-centering at the A and B site of the

octahedral inorganic structure, which causes phase transformation to result in high temperature cubic, tetragonal, and a low temperature orthorhombic–phases (Figure 2a). This happens owing to the occurrence of two types of octahedral rotation: in-phase and out-phase rotations (Figure 2b) [93]. The cubic aristotype structure happens at a higher temperature, but tetragonal, orthorhombic, and monoclinic phases occur at a lower temperature. This leads to lattice dynamics, resulting in phase diversity [94].

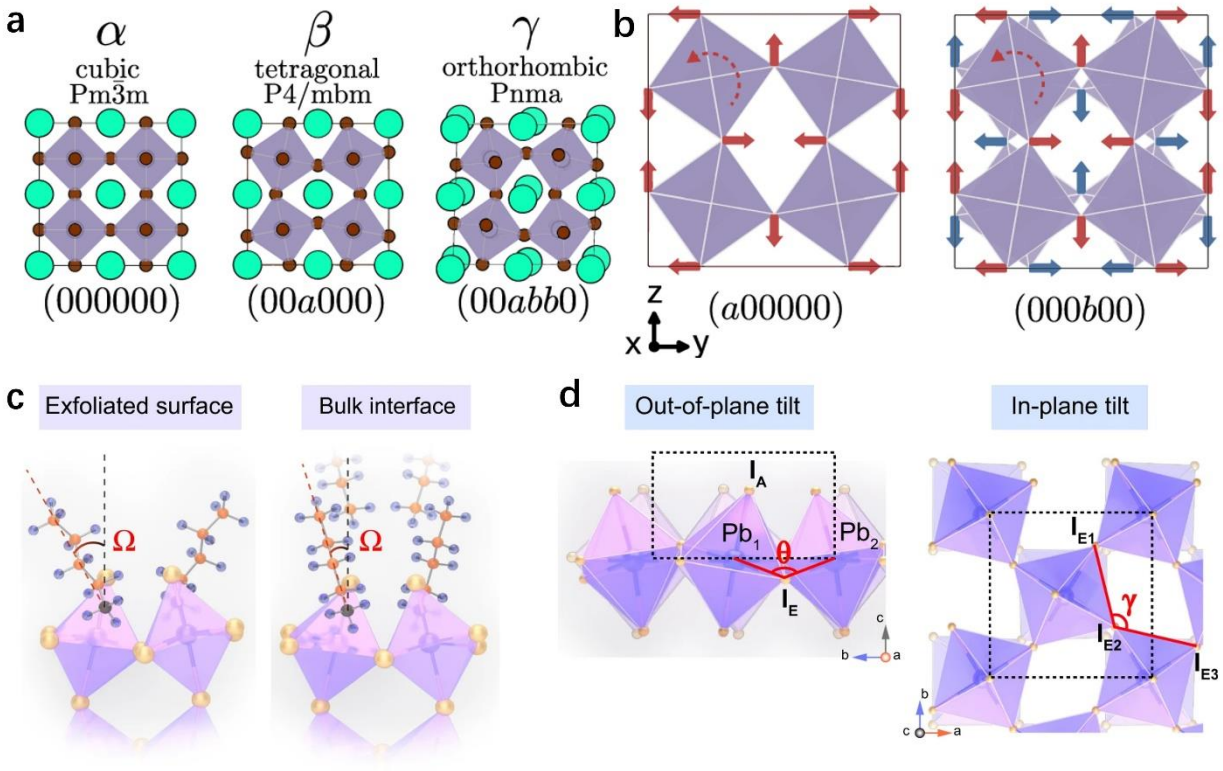

Figure 2. (a) Three types of phases, and (b) in-phase and out-phase rotations (Reproduced from Ref. [93] with permission). Unlocking surface octahedral tilt: (c) exfoliated monolayer surface and bulk interface and (d) out-of-plane and in-plane tilt (Reproduced from Ref. [95] with permission).

To understand the surface structure relaxation process in organic inorganic hybrid 2D perovskite, Yan Shao et al. studied how to unlock the surface octahedral tilt in Ruddlesden-Popper perovskites [95]. The result indicated that surface-enhanced octahedral tilt is correlated with excitonic redshift, which enhances inversion asymmetry normal to the direction of a quantum well and promotes Rashba spin splitting for n > 1. The surface structure relaxation is related to the exfoliated monolayer surface and bulk interface (Figure 2c) while the surface-enhanced octahedral tilt is related to a rotation of the anion cage classified as out-of-plane and in-plane tilt (Figure 2d). Furthermore, the characteristic inorganic octahedral tilt affects the optoelectronic properties such as charge carrier lifetime and band gap [96]. This long charge carrier lifetime in halide perovskite is owing to the presence of octahedral tile, related to dynamic disorder, which impacts the optoelectronic performance [97].

6. Energy applications of halide double perovskites

The key point that researchers deal with regarding materials property is to obtain promising material property for certain promising applications [20]. Thus, many researchers are working on the halide double perovskites for some applications [98] because these materials show promising solar cell absorbers [20,99], tandem solar cells [32,99,100], photocatalytics [20,27,101–103], and light emission devices [20]. Moreover, the applications of halide double perovskites for energy storage systems such as batteries have shown promising research progress [104–107]. In this regard, vacancies are observed to facilitate ion conductivity, surface area, and ion migration, which are vital to energy storage systems such as batteries [108]. Furthermore, MA_2SnCl_6 as a cathode demonstrates the highest specific capacity of 589.98 $mAh \cdot g^{-1}$ while $Cs_2NaBiCl_6$ as an anode demonstrates over 99% Coulombic efficiency with a specific capacity of about 300 $mAh \cdot g^{-1}$[105]. Thus, $Cs_2NaErCl_6$: Li^+ as the negative electrode achieves a coulomb efficiency of nearly 100% with specific capacity of 120 $mAh \cdot g^{-1}$ at 300 $mA \cdot g^{-1}$ after 500 cycles [107]. Although it is believed that halide double perovskites are suitable for energy storage systems such as batteries, research will continue to confirm whether this progress is confidential enough to use them in batteries in the practical work. Until this practical application of halide double perovskites is confirmed, this application will be debatable in the research world. Another application of halide double perovskites such as the $Cs_3Bi_2Cl_9$ electrode for thin film based supercapacitor achieved a higher specific surface area (26.4 $m^2 \cdot g^{-1}$), areal capacitance of 64 $mF \cdot cm^{-2}$, and 6.6 $\mu Wh \cdot cm^{-2}$ energy density much higher than the lead-based devices [109]. With this perspective, halide double perovskites have achieved many possible applications but limited research in fuel cell applications. Hence, new possible breakthroughs are expected to become great research news for the proposed fuel cell applications. Furthermore, X-ray detectors require high sensitivity and acceptable doses applied in security screening, nondestructive industrial inspection, and imaging [110]. Moreover, imaging and self-powered X-ray detection use halide double perovskites such as $Cs_2AgBiCl_6$ with a limit of detection of 241 $nGy \cdot s^{-1}$ and sensitivity of 325.78 $\mu CGy \cdot air^{-1} \cdot cm^{-2}$ [111]. Valuable characteristics such as lower trap density (1.18×10^9 cm^{-3}), high carrier mobility-lifetime product (5.36×10^{-4} $cm^2 \cdot V^{-1}$), and the high dark resistivity (3.1×10^{10} $\Omega \cdot cm$) presented in halide double perovskites make them possible candidates for X-ray detector applications [111]. Finally, opportunities and challenges remain that are addressed elsewhere for possible application of halide double perovskite materials in X-ray detectors [112].

7. Challenges in lead and tin free all-inorganic halide double perovskite solar cells

As a result, revolutionary advances have been claimed in lead halide perovskite photovoltaic, i.e., PCE has reached greater than 24.2% [30] for a single junction organic inorganic halide perovskite in only a few years of development [61,113,114] and 29.15% for a textured monolithic perovskite/silicon tandem solar cell [31], rendering lead halide perovskites a unique type of material for solar energy capture; however, the record for lead free all inorganic halide perovskite is 7.11%, and for both lead and tin free all inorganic halide double perovskite solar cells, the record is 2.8% [33] and 3.3% [43,115] ,which is far less than 24.2% for a single junction and 29.15% for a tandem solar

cell. Unlike their encouraging efficiency, lead and tin based perovskite solar cells face both the toxicity of Pb metal and device instability [47,116,117], which limits the practical applications. Consequently, a great deal has been dedicated to find alternative perovskite materials such as lead and tin free halide double perovskites and lead and tin free all inorganic perovskites [118–121]. The great opportunity to use double halide perovskites is because of the following important points [122,123]: (1) more stable to moisture compared to (MA)PbI_3. A 30-day exposure to 55% humidity [99] causes no decomposition in the material, whereas (MA)PbI_3 is mostly converted to PbI_2 [20,124]. (2) Halide double perovskites are more stable to heat compared to (MA)PbX_3. Volatile organics in (MA)PbX_3 perovskites leave the material at low temperatures. Although $CsPbI_3$ is more thermally stable, it does not form a 3D perovskite under ambient conditions. In contrast, the Bi-containing perovskites can be heated to 350 °C without decomposition [28,125,126]. Furthermore, (3) long photoluminescence lifetimes (660 ns), which are very promising for solar-cell applications and band gap, are ideal for pairing with Si absorbers in a dual-absorber tandem solar cell [125]. On the other hand, halide double perovskites have challenges relating to their physical chemistry and chemical physics, to date, which need further investigations for more advancement. The big challenge in halide double perovskites is a larger band gap causing poor light absorption and low efficiency. This creates a big question and concern that can cause $A_2B^IB^{III}X_6$ based lead-free double perovskites solar cells to be an acceptable alternative to replace organic inorganic halide perovskite solar cells in the market in order to realize the practical applications [127–129]. The key challenging mechanisms during performance improvements are suggested as follows, which will be considered core ideas for advancement. These forward-looking points of discussion are expected to improve the photovoltaic performance in addition to the questions raised elsewhere [128].

7.1. Discouraging power conversion efficiency

Regardless of the quick development of halide double perovskite solar cells, the cell power conversion efficiency remains about 2.5%, which was achieved using $Cs_2AgBiBr_6$ [33] and 3.3% using Cs_2TiBr_6 [43]. Furthermore, the strategy to improve both material and device efficiency made of these materials becomes a great concern. Moreover, looking at halide double perovskite light absorbers of high-quality with high absorption coefficient, longer diffusion length, and free of defects, trap states with less radiative centers are concerning. In accordance with the Shockley-Queisser limit, a theoretical maximum PCE of 16.4% can be obtained with an E.g. of 2.2 eV, thus holding promise for working double perovskite based photovoltaics [129]. Even though the theoretical maximum PCE of $Cs_2AgBiBr_6$ does not reach the highest reported PCEs of single-junction $MAPbI_3$-based photovoltaic cells, $Cs_2AgBiBr_6$ is a promising candidate for applications in tandem solar cells, as was already shown for $MAPbBr_3$, which features a slightly larger E.g. of 2.3 eV [130]. Not only are the energy alignment and band gap with the charge extraction layers important, but the charge collection efficiency is vital to manufacture high-efficiency solar cells [40].

7.2. Mismatch among various interfacial layers of the device architecture

This is another key challenge in halide double perovskite solar cells that remains an unexplored area of research. Furthermore, poor interfacial integration might lead to broadening of the depletion width, poor band alignment, inefficient charge collection, enhanced recombination, insufficient charge transport, and poor overall device performance. For instance, such mismatch in energy levels has occurred in materials such as $(MA)_2AgBiI_6$ and Cs_2PdBr_6. For example, $(MA)_2AgBiI_6$ was observed as not compatible with TiO_2 but was well-matched with SnO_2 and C_{60} [131].

7.3. Unclear charge-transport properties of these materials

Whether or not they are as favorable as lead-based perovskites is not well known. The optoelectronic properties of $Cs_2AgBiBr_6$ and $Cs_2AgBi_{1-x}SbxBr_6$ have displayed a comparable rate-transport mechanism, which can act as an alternative absorber to lead-based perovskites [15]. The charge carrier density of both $Cs_2AgBiBr_6$ and $Cs_2AgBi_{1-x}Sb_xBr_6$ is limited to 10^{16} cm^{-3} and a mobility of 0.8 cm^2/Vs as well as tunable band gap of 2.0 to 1.6 eV [132,133]. Thus, this charge transport property requires greater attention for further improvement of the field. The carrier mobility of $Cs_2AgBiBr_6$ is 0.3–11 cm^2/Vs with electron and hole mobility of 17 and 14 cm^2/Vs, respectively [134]. Other charge transport properties of $Cs_2AgBi_{1-x}Sb_xBr_6$ have not been reported. Thus, further study is required to clarify and fill the limitation not yet reported.

7.4. Quantum confinement effect

The quantum confinement effect in the last shells due to restricted orbital interactions of the adjacent cations, particularly B′ and B″ cations in the cubic unit cell of the $AB'B''X_6$ double halide perovskite materials, might result in a narrow and localized conduction band edge as well as a broad energy gap, which deteriorate the device performance [27,127]. Consequently, finding a way to move into another unite cell structure is expected to overcome such challenges.

7.5. Low electronic dimensionality

Halide perovskites have both low and higher dimensionality. Such dimensions have their own electronic and optical properties that impact the efficiency and stability of halide perovskites. This structural dimension at the molecular level ranges from 0D to 3D (Figure 3, Table 1), where D stands for the word ‘dimension’. High dimensionality, i.e., 3D lead halide perovskites, achieved high performance. The majority of these materials demonstrated 3D dimensionality [28]. On the other hand, halide double perovskites showed broad band gaps, which means structural dimensionality is a factor affecting PCE in addition to the electronic band gap that is affected by the electronic dimensionality. This might make halide double perovskites inappropriate for a single junction solar cell function though these materials crystallize into 3D [119]. Furthermore, the most explored halide perovskite are 2D and 3D, while those least explored are 0D and 1D. The reason why they are unexplored lower dimensional halide perovskites is because of site isolation and strong confinement [135].

Table 1. Comparison of 0D, 1D, 2D, and 3D halide perovskites.

Properties of low and high dimensional structures			
0D [136]	1D [137,138]	2D [139–141]	3D [142–144]
• Individual metal halide octahedral anions or metal halide clusters are completely surrounded and isolated by the organic cations. • Molecular perovskite units are embedded in the crystal lattice. • General chemical formula is A_4BX_6, where a represents monovalent organic cations and BX_6 represents metal halide octahedra. • Weaken the light absorption range and hinder charge transport.	• The metal halide octahedral are corner-sharing, edge-sharing, or face-sharing to form a 1D nanowire. • Either linear or zigzag configurations. • Chemical formulas are variable depending on the connecting methods and the organic cations chosen. • Weaken the light absorption range and hinder charge transport. • High stability of low dimensional perovskites.	• High stability of low dimensional perovskites. • Suppress moisture invasion. • Prevent moisture intrusion. • Improve thermal stability. • Suppress ion migration. • The links between octahedra $[BX_6]_4-$are separated by large organic cations along crystallographic planes. • The chemical formula is generally described as $(A')_m(A)_{n-1}B_nX_{3n+1}$. • The 2D perovskite is more stable than its 3D phases. • 2D perovskite-based PSCs do not exhibit ideal performance due to their larger bandgap, low carrier mobility and weaker carrier transport resulting from insulating spacer cations.	• Superior efficiency of 3D perovskites. • Consists of a network of corner-sharing BX_6, where the B atom is a divalent metal cation (typically Ge^{2+}, Sn^{2+} or Pb^{2+}) and X is a monovalent anion (typically Cl^-, Br^-, I^-). • Sensitive to moisture invasion. • Does not prevent moisture intrusion. • The chemical formula is generally described as ABX_3. • The 3D perovskite is more unstable than its 2D phases. • 3D perovskite-based PSCs exhibit ideal performance due to their narrow band gap, high carrier mobility and stronger carrier transport resulting from insulating spacer cations.

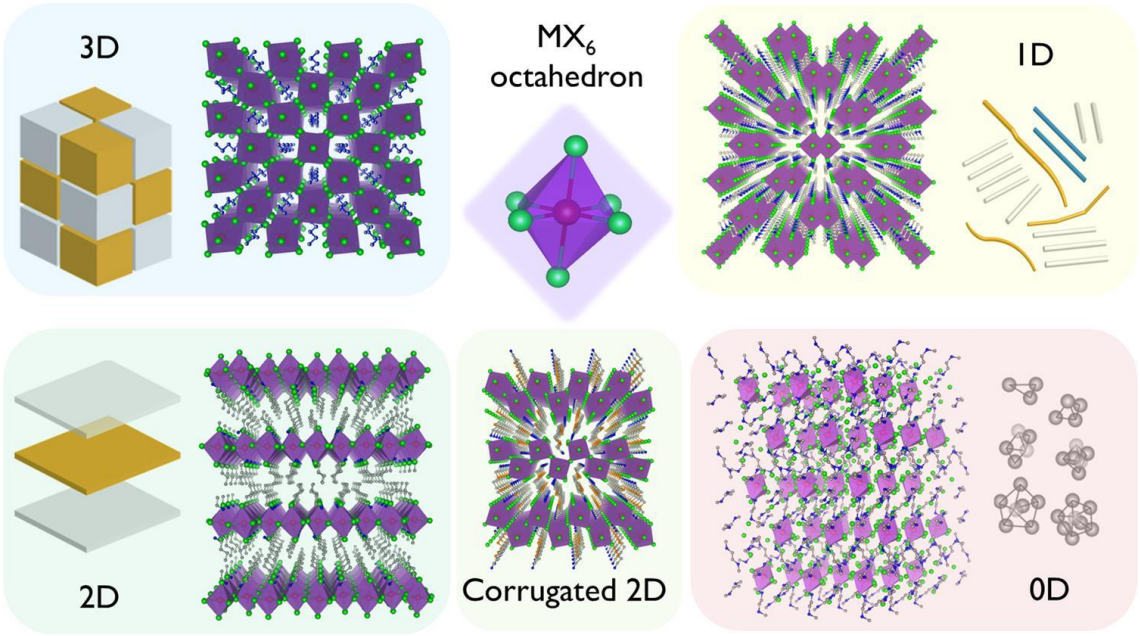

Figure 3. Illustration of perovskites: low and high dimensional structures (Reproduced from Ref. [135] with permission).

7.6. Indirect and wide band gaps

The higher performance of organic, inorganic halide perovskites was achieved due to their direct and lower band gap, but halide double perovskites possess indirect and wide band gaps which limit the absorption of light for solar cells and is not ideal for thin film PV applications cases, and this field needs band gap engineering. For instance, in recent times, bismuth and silver based perovskites were anticipated as a choice to replace $MAPbI_3$ [51,125]. The band gaps are indirect, which is not ideal for single junction solar cell applications, though bismuth/silver based double perovskites absorb 1.9 to 2.2 eV [145]. The reason that indirect semiconductors are not preferable compared to direct semiconductors is due to the weak oscillator strengths for radiative recombination and for optical absorption, which might be a challenge if there is low carrier mobility. Similarly, $Cs_2AgBiBr_6$ has a 1.95−2.19 eV indirect band gap [146–147], showing a comparable lifetime with optimized lead halide perovskite films [148,149]. Solving the issue of non-radiative recombinations from its indirect band gap makes them promising for photovoltaic application. The charge mobility in the polycrystalline $Cs_2AgBiBr_6$ is 1 $cm^2 \cdot V^{-1}s^{-1}$ [135], while in the single crystal it is 11.81 $cm^2 \cdot V^{-1}s^{-1}$, indicating that charge transport property is superior in single crystals.

7.7. Energetic disorder

The energy state of a given semiconductor is described via energy disorder since it impacts charge transport, carrier mobility, and recombination rate [117,150]. Such disorder may be dynamic (caused by carrier phonon interactions) and/or static (caused by impurities or defects) disorder, which influence inter-band structure as shown in Figure 4 [151]. In organic solar cells,

energetic disorder is caused by the synergy of intra- and intermolecular interactions that originated from intermolecular disorder, the unfavorable molecular packing behavior [152]. In mixed halide perovskites, the origin of the disorder would be compositional disorder causing inhomogeneity of halide ions [153,154]. The great debate here is: which type of energy disorder matters for carrier recombination dynamics, charge transport, band-tail structure, carrier mobility, carrier trapping, and ultimately device performance? Thus, understanding energetic disorder in halide double perovskites becomes necessary of the time scales connected with atomic and molecular motions as well as the variation of the disorder from a single crystal to the thin film [155]. Knowing the variations might also be vital during the processing of these light-absorbing materials and hence strongly correlated with the device performance.

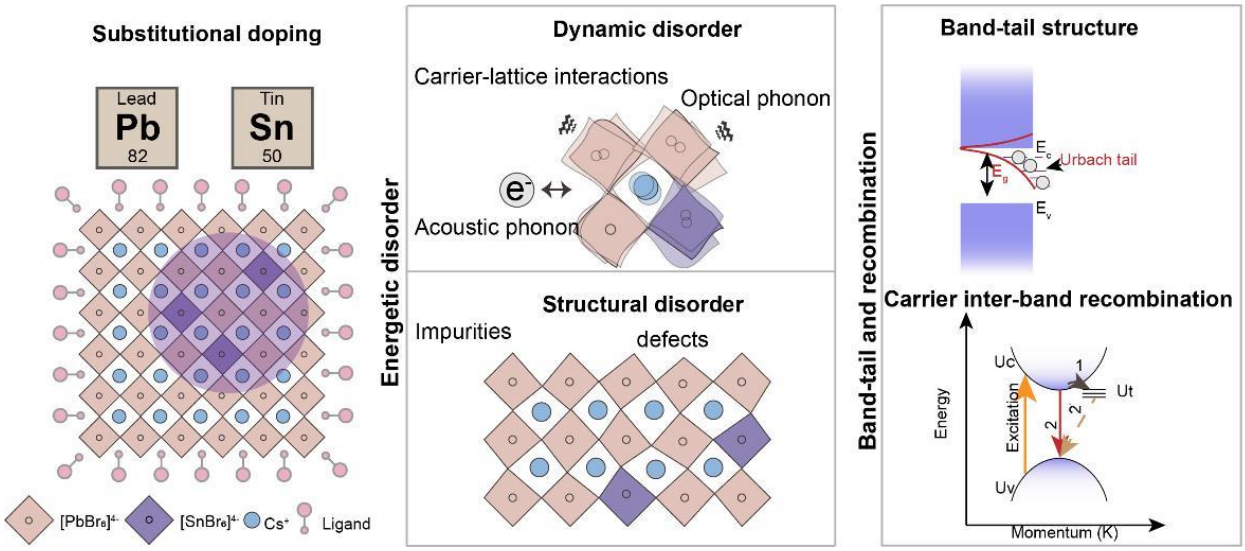

Figure 4. Impact of energetic disorder in $CsSn_xPb_{1-x}Br_3$ based perovskite solar cells (Reproduced from Ref. [151] with permission).

7.8. Geometrical constraints

There are variations reflecting the coordination and local chemistry. As these uncertainties transfer to the octahedral and tolerance factors, the stability ranges proposed so far are descriptive rather than predictive. There are some geometric factors restricting the formation of stable 3D halide double perovskites. Many promising routes towards Pb-free halide double perovskites have been explored to replace Pb by elements such as germanium [74], bismuth, or antimony and noble metals [126,131]. However, the geometrical constraints imposed by the necessity of forming an ideal perovskite lattice, in addition to the common oxidation states of these optional cations (e.g., +3 of Bi and Sb), still cause this to be a difficult discovery of lead-free materials that could rival the optoelectronic properties of prototypes such as $MAPbI_3$.

7.9. High processing temperature

While organic inorganic halide perovskites need annealing temperatures usually less than 100 °C, the halide double perovskites are fabricated only at a higher annealing temperature up to 285 °C [40,156]. Such prerequisites for fabrication might damage the integration of the device architecture and further restrict wide range function of these materials. Additionally, such high energy consumption for materials fabrication is not economically cost-effective, environmentally none green, and is not sustainable. As a result, looking for alternative methods that could minimize such higher processing temperature becomes an impressive research area in this field.

7.10. Shortage of a broad-spectrum of speculative guidelines

In spite of considerable contributions, there is no well-refined guideline and theoretical understanding for what kind of mixed B-site cation halide double perovskites should be used and how to design Pb and Sn free halide double perovskites for enhancing collective optical, electrical, thermal, and mechanical properties and long term stabilities of these materials for wide range applications. In order to minimize such bottleneck challenges, detailed knowledge of the electronic structures of these materials with respect to B'/B" cation arrangement and design become attractive research directions in the field of halide double perovskites.

7.11. Lack of stoichiometric design and compatibility of various layers

Stoichiometric design of the perovskite [156] has been known as a strategy to develop solar cells with enhanced performance. Moreover, unique stoichiometric design and compatibility of various interfacial device layers are essential aspects that require more attention [19,26,157].

7.12. Incomplete order

Elucidating the arrangement and position of the ions is another concern in halide double perovskites. Because the B cations generally determine the physical properties of double perovskites, there are three B-cation sublattice types known for double perovskites: random, rock salt, and layered. The latter two are ordered arrangements. In some situations, it is observed that the order is not complete, especially in the $A'A''B'B''X_6$ structure. Interestingly, order-disorder effects are mainly encountered when the charge variation between B' and B" is two or less. Although the degree of order is an important subject, the dynamic nature of order-disorder behavior is a quite useful parameter [11,46,158,159].

7.13. Challenges in achieving high quality films

Unlike organic inorganic halide perovskites, achieving high quality film in halide double perovskites becomes a challenge. High quality film might be defined as a material with excellent crystallinity, uniform morphology, less defects, high absorption coefficient, superior ambipolar

carrier transport ability [160], and high coverage or pinhole-free film [161,162]. All these parameters are well known to deter both materials and device performance in halide double perovskite solar cells if the quality of these materials is not well optimized during processing steps. For that reason, the light harvesting and active layer that is the halide double perovskite monolayer in the perovskite solar cells is one of the very important research topics that researchers deal with. Moreover, controlling and designing the colloidal properties of the precursor and solvent engineering [60,163,164] should get considerable attention to enhance the required film with high quality [165–167].

8. Suggested research roadmap engineering strategies for material and device performance improvement

In order to overcome the key challenging mechanisms faced by halide double perovskite solar cells, suggesting key areas of research that will be considered as research roadmap for improvement of both material and device performance is quite important. These include engineering microstructure, surface and bulk properties, grain boundary and domain wall engineering, polar order engineering, band gap and band structure engineering, colloidal engineering, composition engineering, optoelectronic engineering, device architectural engineering, interface and defect engineering, equilibrium and non-equilibrium quantum transport, and ferroelectric engineering, as shown in Figure 5.

Figure 5. Suggested research roadmap for performance improvement in lead and tin free halide double perovskite solar cells.

8.1. Engineering materials microstructure, surface, and bulk properties

Engineering microstructure, surface, and bulk properties of halide double perovskites are important mechanisms and research areas for improvement for both materials and devices [20,50,124,168,169]. Microstructure influences virtually all aspects of the behavior of materials. Moreover, it is the spatial distribution of material in the useful object that is the goal of the endeavor and is the most richly variable; thus, this is the most susceptible to control of the elements in the materials structural hierarchy. Engineering microstructure of materials [168,170] comprises the concepts of morphology or topological properties and geometry, thermodynamic properties, surface and bulk properties, and grain growth as well as bulk and nano-scale domain structures.

8.2. Engineering domain wall and grain boundaries

The halide double perovskite microstructure might offer optional lanes for conductivity and electron−hole disjointing. Because grain boundaries have an impact on the long-term stability along with the ferroelastic domain boundaries that might be different from regular grain boundaries, the finding of ferroelasticity offers a novel parameter to pursue in favor of enhancing their stability as well as facilitating their extensive implementation [171]. Additionally, grain engineering and morphology control through the introduction of additives to the perovskite precursor is another way for performance improvement [31]. Sub-micron-sized crystal grains in perovskite thin films, on the other hand, have been obtaining considerable attention due to their fundamental morphological properties in the course of twin domains [172,173], which are highly essential for understanding the basic mechanisms, for instance, of low recombination rate and long diffusion length of the device's high performance [174]. Moreover, the presence of charged domain walls will significantly reduce the band gap by 20%−40% and can serve as segregated channels for the motions of charge carriers, while the presence of uncharged domain walls has no substantial impact on the band gap [175].

8.3. Polar order engineering

Effect of polarization, molecular dipoles, tilting of octahedron and transition metal cation size, and its oxidation states on photo-excitation, band structure, and photoluminescence are not well investigated. Notwithstanding the microscopic model, polar order is accepted to recline at the center of the ferroelectric photovoltaic impact [176]. Besides, it is outstanding that interactions between lattice, orbital, and polarization order parameters in ferroelectric materials initiate upgrades of their physical properties close to phase boundaries [177]. On the road to advanced performance, conventional approaches focus on reducing the band gap to superior fit the solar spectrum, while reducing the basic relation between polar order and photovoltaic effect is ignored [177]. Hence, spotlighting both narrowing the band gap and basic relation between polar order and photovoltaic effect has become an attractive research topic.

8.4. Band gap and band structure engineering

The fundamental bottleneck restraining the function of halide double perovskites is their bigger energy gap. The most favorable band gap for the single junction solar cells ought to be close to 1.3 eV [178]. As a result, band gap and band structure engineering are vital if halide double perovskites are to be suggested optional contender materials as shown in Figure 6. On the other hand, $Cs_2Ag_{0.95}Ga_{0.05}BiBr_6$ based double halide peroveskite solar cells show a small performance improvement of 4.52% via band gap reduction [179]. If the suggested engineering strategies are implemented, it is promising to maximize the power conversion efficiency of these solar materials.

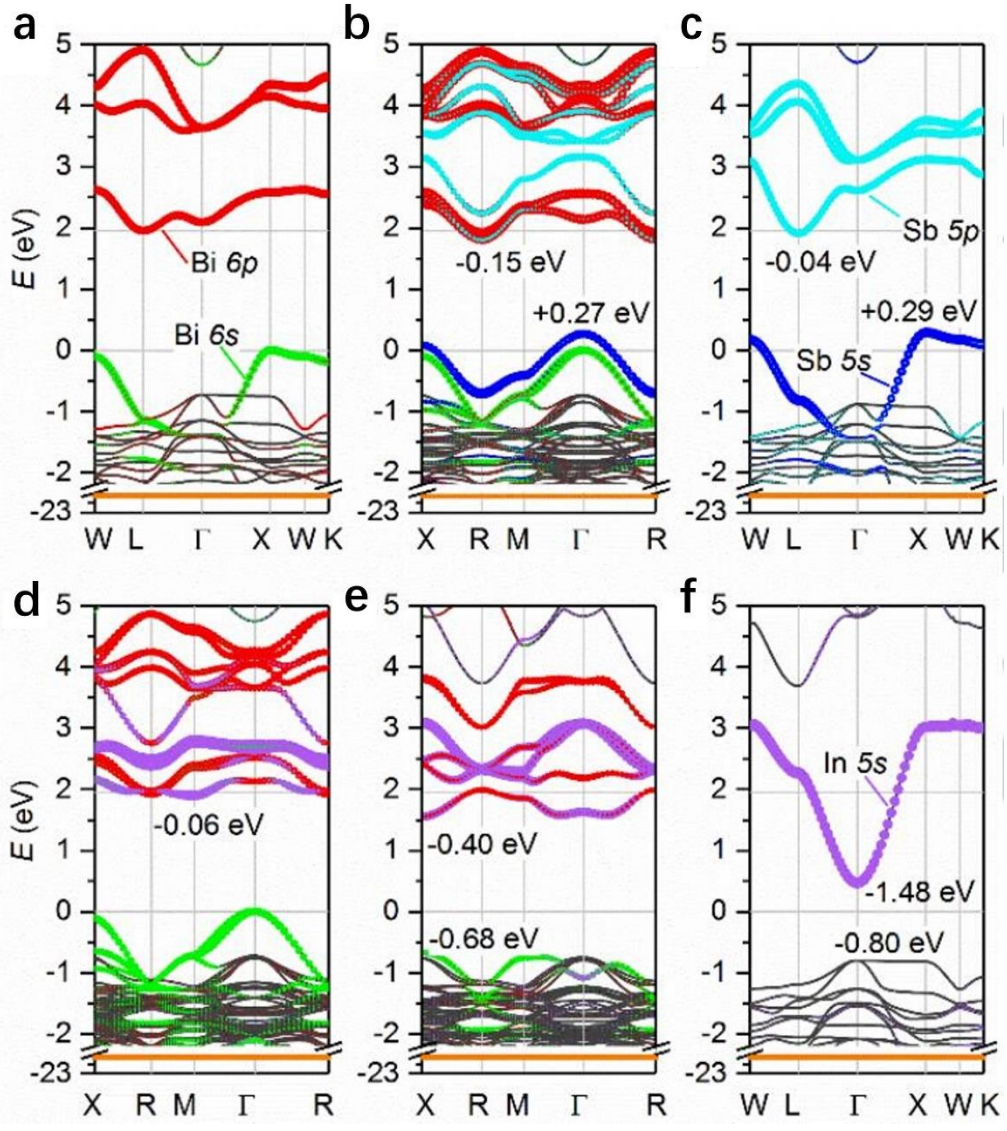

Figure 6. Band gap and band structure engineering: band structure of (a) $Cs_2AgBiBr_6$, (b) $Cs_2AgBi_{0.75}Sb_{0.25}Br_6$, (c) $Cs_2AgSbBr_6$, (d) $Cs_2AgBi_{0.75}In_{0.25}Br_6$, (e) $Cs_2AgBi_{0.25}In_{0.75}Br_6$, and (f) hypothetical $Cs_2AgInBr_6$ (Reproduced from Ref. [180] with permission).

As shown in Figure 6, the band gap and band structure of various $Cs_2AgBiBr_6$ derivatives are shown as indirect band gap semiconductor materials, substituting Bi using Sb and In elements. Bi 6p orbitals are the conduction band minimum for $Cs_2AgBiBr_6$ (Figure 6a), while the Bi 6s orbitals construct their valence band maximum with a calculated indirect band gap of 2.0 eV. Furthermore, a valence band maximum is constructed by the Sb 5s orbital observed above the Bi 6s orbitals for $Cs_2AgBi_{0.75}Sb_{0.25}Br_6$ (Figure 6b) whiles its conduction band minimum is constructed from the Sb 5p orbital. The 1.58 eV indirect band gap is obtained from this calculation. The conduction band minimum for $Cs_2AgSbBr_6$ is derived from Sb 5p orbitals, but its valence band maximum is derived from Sb 5s orbitals (Figure 6c) with a calculated band gap of 1.67 eV. Further substitution with In metal results in a new band structure, introducing 4s orbital in the lower conduction band, but Bi 6s orbitals drives the valence band maximum with an indirect band gap structure. Thus, a larger band gap of 2.28 eV has been calculated for $Cs_2AgBi_{0.25}In_{0.75}Br_6$ (Figure 6d,e), which is larger than that of $Cs_2AgBiBr_6$. Increasing In concentration leads to strong coupling in the [$InBr_6$] octahedral, resulting in a reduced gap caused by the In 5s-derived conduction band. These band structures obtained by Sb and In atomic substitution suggest that every atom introduced has its own band structure and unique optoelectronic properties with unique optical and electrical performance. Thus, understanding band structure matters for optoelectronic properties and the application of a given semiconductor.

8.5. Crystallization process and colloidal engineering

The nucleation and growth, coordination chemistry, and coordination engineering of halide double perovskites need to be studied: In addition to the photophysics properties, the nucleation and growth, coordination chemistry, and coordination engineering concepts are equally important and quite essential for developing new halide double perovskite materials [181]. Therefore, colloidal engineering, colloidal chemistry, and ion exchange reactions during synthesis of halide double perovskites are important ideas that need to be controlled for synthesizing high quality thin film for high performance.

8.6. Composition engineering

The computational details on the structure of $Cs_2AgBiBr_6$ double perovskites were reported recently, as shown in Figure 7a,b [182]. This structure is taken as the starting material for its derivatives such as $Cs_2AgSb_{0.5}Bi_{0.5}Br_6$, $Cs_2Ag(Bi_{1-x}Tl_x)Br_6$, etc. From these reports, $Cs_2AgBiBr_6$ crystalizes as a face-centered cubic structure with a space group of *Fm*3m, as shown in Figure 7a. The atomic positions of the Ag atom is at (4a) (0,0,0), Cs atom is at (8c) (0.25, 0.25, 0.25), Br is at (24e) (ux, 0, 0), and Bi atom is at (4b) (0.5, 0.5, 0.5). Its tetragonal structure (Figure 6b) crystalizes at low temperatures with the atomic position of Br_2 atom at (4e) (0, 0, uz), Br1 atom at (8 h) (ux, uy, 0), Ag atom at (2b) (0, 0, 0.5), Bi atom at (2a) (0, 0, 0), and Cs atom at (4d) (0.5, 0, 0.25) [182]. Furthermore, the band structure of $Cs_2AgBiBr_6$ with an indirect band gap character is shown in Figure 7c,d. The band edges are mostly formulated from Br, Bi, and Ag states. The Bi–p states contribute to the conduction band while Ag–d and Br–p hybridized states contribute to the formation of a valence band. The band edges are made of Br, Bi, and Ag states. Bi–p states contribute to the

formation of conduction bands while Br–p and Ag–d hybridized states contribute to the formation of valence bands. The possible electron transition occurs in Ag–s and Bi–p antibonding states from Br–3p and Ag–4d bonding. Thus, the optoelectronic properties of $Cs_2AgBiBr_6$ are influenced by Ag, Bi, and Br atoms. Furthermore, all possible compositional displacements and addition of atoms at a given ratio can take place at these atoms for possible modifications of the electrical and optical properties as well as other applications.

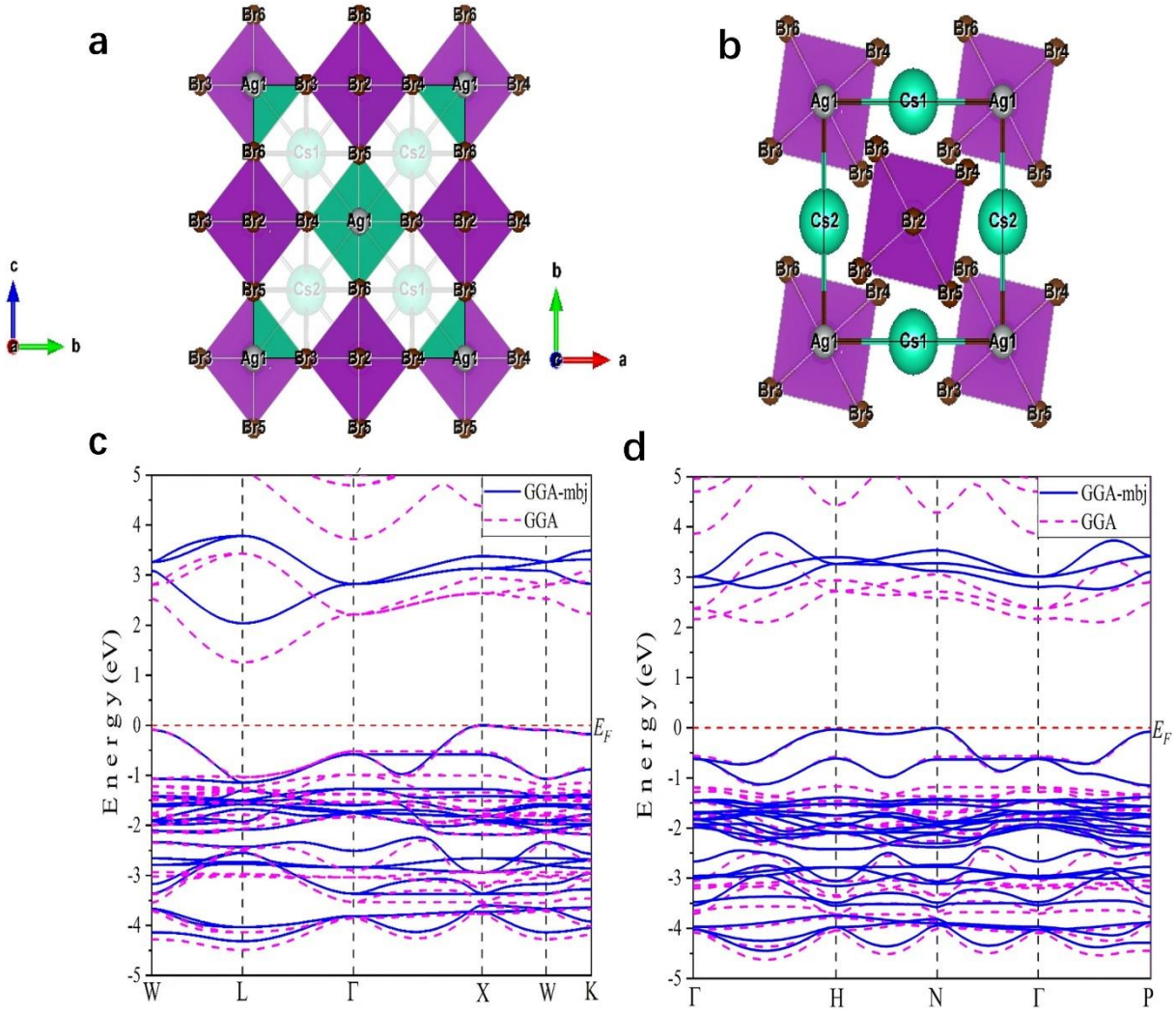

Figure 7. Crystal structure of (a) cubic and (b) tetragonal phases of halide double perovskite $Cs_2AgBiBr_6$, and the band structures for (c) cubic and (d) tetragonal phases (Reproduced from Ref. [182] with permission).

Cation and anion displacement, cation-anion order-disorder effects, cation size mismatch, distortion, tilting, ordered vacancies, hydrogen bonding, charge disproportionation, and stereochemistry or lone pair effects need to get more attention in order to improve stability, inferior material, device performance, and engineering a new halide double perovskite material [13,119,152–154]. In addition, the creation of new chemical compositions using new elements in the mixed halide double perovskite structure is an acceptable strategy to tune the band gap and other optoelectronic properties [183].

Currently, $Cs_2AgBiBr_6$ and Cs_2TiBr_6-based lead and tin-free all-inorganic halide double perovskites are reported as alternative types of perovskite solar cells. The latter has an energy gap of 1.8 eV in addition to its >100 nm carrier diffusion length [43]. The composition engineering due to modifications at the halide anion from Br to I results in the reduction in band gap ranging from 1.8 to 1.0 eV [37]. This band gap is suitable for single junction halide double perovskite solar cells [37]. Furthermore, modifications at the cation site, A-site, and B site are not confirmed. Similarly, $Cs_2AgBiBr_6$ has a high band gap, tunging from 1.83 to 2.21 eV [125,40,184]. Composition engineering at the A, B, and X sites may reduce the band gap to make it more suitable for single-junction halide double perovskite solar cells [185]. Recently, precursor engineering has been suggested as a route to enhance the power conversion efficiency of $Cs_2AgBiBr_6$ materials, showing 40% enhancement [186]. This result indicates that precursor engineering is one type of composition engineering that is responsible for obtaining smooth, large grains, and high-coverage $Cs_2AgBiBr_6$ films.

The indirect band gap characteristics of the inorganic double perovskite band structure have been reported as shown in Figure 8 [77]. In this report, pure Sb($Cs_2AgSbBr_6$, $Cs_2AgSb_{0.5}Bi_{0.5}Br_6$) and pure Bi($Cs_2AgBiBr_6$) double perovskites have been studied (Figure 8). Electronic band structures were computed employing the TB09 method, considering both the inclusion of spin–orbit coupling (depicted by the black lines) and its exclusion (represented by the red lines). Materials under investigation include pure Sb alloy $Cs_2AgSbBr_6$ (Figure 8a), mixed alloy $Cs_2AgSb_{0.5}Bi_{0.5}Br_6$ (Figure 8b), and pure Bi alloy $Cs_2AgBiBr_6$ (Figure 8c). The valence band maximum (VBM) of these three compounds is situated at the X point, whereas the conduction band minimum is positioned at the L point in the reciprocal space. This observation signifies the indirect band gap nature of these compounds. Band gaps obtained from calculation inclusion with SOC are lower than that of exclusion with SOC. This results from SOC leads to band degeneracy resulting in a reduction of the band gap. Band gaps calculated with the inclusion of SOC are lower than those obtained without SOC. This discrepancy arises because SOC introduces band degeneracy, consequently decreasing the band gap in these systems. Indirect band gaps calculated by TB09-PBE (excluded SOC) of pure $Cs_2AgSbBr_6$, mixed $Cs_2AgSb_{0.5}Bi_{0.5}Br_6$, and pure $Cs_2AgBiBr_6$ are 1.69, 1.96, and 2.17 eV, respectively.

The indirect band gaps of 1.69, 1.96, and 2.17 eV are reported for pure $Cs_2AgSbBr_6$, mixed $Cs_2AgSb_{0.5}Bi_{0.5}Br_6$, and pure $Cs_2AgBiBr_6$, respectively [77]. The conduction band of these materials is dominated by the Ag–d orbitals while the valence band is dominated by Sb–p orbitals in pure $Cs_2AgSbBr_6$ and $Cs_2AgSb_{0.5}Bi_{0.5}Br_6$ but Br–p orbitals in pure $Cs_2AgBiBr_6$ [77]. Hence, it is possible to investigate photoactive materials for various applications as a function of compositional engineering in the field of lead-free halide perovskite materials.

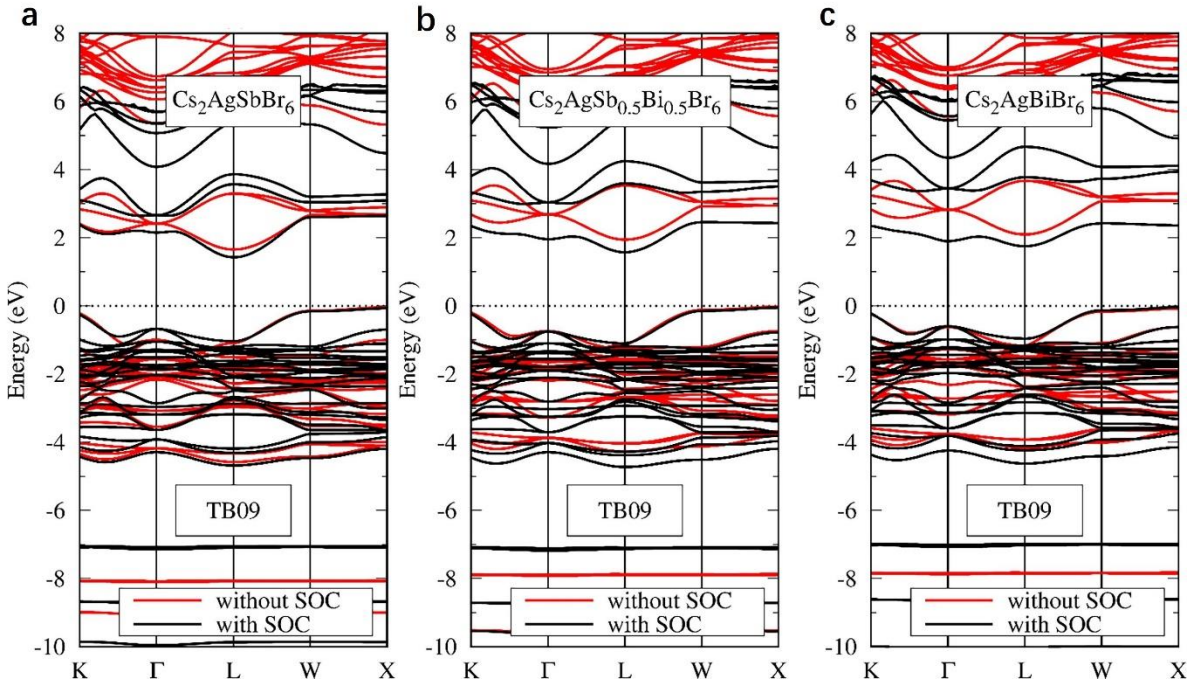

Figure 8. Electronic band structures were computed using the TB09 method, both with spin–orbit coupling (indicated by black lines, with SOC) and without spin–orbit coupling (indicated by red lines, without SOC) for (a) a pure Sb alloy $Cs_2AgSbBr_6$, (b) a mixed alloy $Cs_2AgSb_{0.5}Bi_{0.5}Br_6$ and (c) a pure Bi alloy $Cs_2AgBiBr_6$, respectively (Reproduced from Ref. [77] with permission).

8.7. Engineering photoelectric properties

Ferroelectrics, dielectrics, piezoelectric, pyroelectrics, electro- and photocatalytic properties, thermoelectric properties, electrical transport properties, and other optoelectric properties have not been studied [11,20,171,187,188]. Optical transition in identical inversion symmetry is symmetry forbidden, leading to poor optical absorption, as shown in Figure 9a [189]. For instance, in $Cs_2AgTlCl_6$ the band gap transition at Γ contains the A_{1g} orbital in the CB and E_g orbital in the VB (Figure 9b) owing to grade symmetry, which results in forbidden band gaps. Furthermore, the optical transition from Γ to L progressively becomes allowed (Figure 9c). Such isoelectronic properties are observed in $Cs_2AgInCl_6$, where Figure 9d shows the formation of a new conduction band owing to increasing Tl^{3+} concentration in $Cs_2Ag(Bi_{1-x}Tl_x)Br_6$. Introducing Tl^{3+} reduces the band gap of $Cs_2Ag(Bi_{1-x}Tl_x)Br_6$ since the $Cs_2AgBiBr_6$ band includes Tl^{3+} 6s orbitals (Figure 9d) [189]. From this perspective, the band structure depends on the composition of metal atoms incorporated in the structure of the semiconductor.

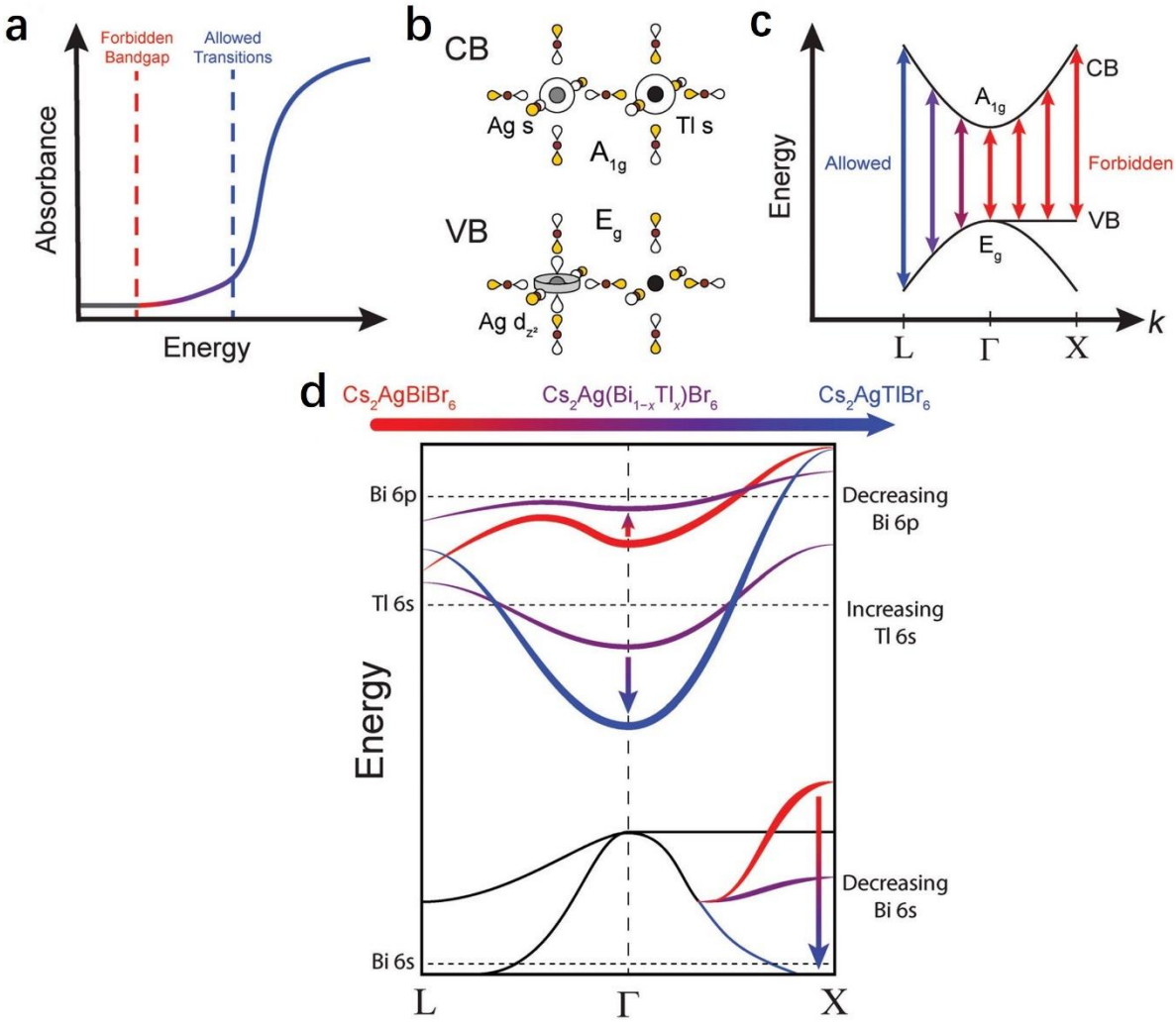

Figure 9. Illustration of symmetry-forbidden band gaps and change in the electronic structure using $Cs_2AgTlCl_6$: (a) the weak absorption onset, (b) schematic orbital representation of the valence band (VB) and conduction band, (c) band diagram depicting allowed and forbidden optical transitions, and (d) the change in electronic structure over the composition range of the $Cs_2Ag(Bi_{1-x}Tl_x)Br_6$ (Reproduced from Ref. [189] with permission).

Moreover, the microscopic physics related properties that mater the photovoltaic effect are vital properties in the field of photovoltaics. This property becomes inadequately known and tarnished when we discover the double perovskite solar cells. Furthermore, diverse methods have been suggested to explain research outputs in a variety of device architectures, such as asymmetric momentum distribution of the non-equilibrium carriers [190,191], shift in current through coherent evolution [192–194], polarization-dependent interfacial band bending [195,196], and bulk depolarization field [195].

From a material properties and applications perspective, understanding and extracting information on the presence or absence of ferroelectrics in halide perovskite materials will greatly contribute to multifunctionalities in the field of electronics beyond photovoltaic; additionally, symmetry and

structure of the crystalline unit cell determines the ferroelectricity of materials [197]. For ferroelectricity to be detected, the primary requirement is the presence of a non-centrosymmetric unit cell. According to the definition of Anderson and Blount [198], a ferroelectric material has to encompass several criteria: (1) a continuous structural transition; (2) a non-centrosymmetric low temperature structure; and (3) a structure with a unique polar axis (a rotational axis of symmetry without a mirror plane perpendicular to it) at low-temperatures [199,200]. All these properties clarify the origin of ferroelectricity [201]. Whether or not a material has such a polar axis is decided exclusively by its crystal structure and creates the delicate variation between pyro- and piezoelectric. $LiOsO_3$, whose existence was first predicted half a century ago [202] has been identified [203] as an example of a ferroelectric metal, and has been established. It is likely that materials in this class could show some attractive physical properties. For instance, at enhanced temperatures, the existence of ferroelectric-like soft phonons can stabilize non-centrosymmetric superconductivity [204].

In addition to this, there are essential situations for bulk ferroelectricity to be present [205]: (1) noncentrosymmetric properties without inversion symmetry; (2) characteristic polarity; (3) an assembly of polar unit cells facing a similar direction that can make a "polar domain"; and (4) polarization switching. In addition to the electrical responses, ferroelectricity can be structurally explained using periodically ordered polar domains. Like the other ferroelectric materials, the relationship between the crystal thickness, D, and domain periodicity, ω, obey the Landau–Lifshitz–Kittle model scaling relationship as $\omega \sim D^{0.6}$ for $MAPbI_3$ perovskites. Due to differences in doping, the crystal synthesis could affect the ω–D relation. Derived from the periodic structure and etching, the domains appear to develop a head-to-head orientation.

Based on these facts, ferroelectricity in halide perovskites remains elusive. Inorganic materials with ferroelectric properties like $BiFeO_3$ have revealed a huge possibility in many other functionalities beyond photovoltaic [206]. At this time, application in optoelectronic devices and the related semiconducting properties of stannate or hybrid organo-plumbate become burning issues. With respect to their structural properties, these materials are appropriate for investigation regarding ferroelectricity [207]. As a result, the architecture of molecular ferroelectric semiconductors based on these materials demonstrates an opportunity to get novel or high-performance semiconductor ferroelectrics. In this section, we will address ferroelectric properties in both halide perovskite and fully inorganic perovskites. Until now, since this is a greatly arguable matter, additional proof for ferroelectricity of the material has to be present and is, therefore, shown. With the application of steady-state conditions, very important points become energetic as follows [205,208]:

(a) Buildup of unlike charged species at the outer surface of the polar bulk (e.g., adsorption of free charges or charged molecules from the adjacent electrodes or environment, respectively). This event, known as "pyroelectricity", is straight confirmation for accessible polarity. Previously, a clear experimental proof demonstrated that at room temperature (RT), cubic $MAPbBr_3$ is not pyroelectric [209]. In addition, it has been evidenced practically that tetragonal $MAPbI_3$, is pyroelectric [205].

(b) Buildup of mobile holes and electrons from the polar bulk material can happen if the bulk materials is adequately conductive, beyond $\sim 10^{-6}$ $S \cdot cm^{-1}$, a sensible value for a low bandgap semiconductor, like that of $MAPbI_3$. Thus, leakage currents ought to govern the dielectric response and are influenced by the bulk overall polarization [205].

(c) Stacking of domains of contrary polarity to reduce Coulomb repulsion, except at the price of creating a "domain-wall". For several famous ferroelectric materials, the periodicity between the domains, ω, scales with the crystal thickness the length of its polar axis, D, as $\omega \sim D^{\gamma}$, where γ is the power reliance that is hypothetically equivalent to 0.5 [210,211]. The tetragonal $MAPbI_3$ follows this rule [205].

(d) Accordingly, the quarrel on ferroelectricity in $MAPbI_3$ has not been concluded with clear termination, which inspires us to review ferroelectric behavior of various perovskite materials such as $MAPbI_3$, $FAPbX_3$, $CsSnI_3$, $RbSnI_3$, and layered and double perovskites in the next subsections.

Domains created by the sharing of spontaneous polarization in space are important to characterize ferroelectric materials. These domains, in a given ferroelectric material, are illustrated in Figure 10. Arrows point out the trend of net polarization in domains and the constituent of the polarization vector. The constituent of the polarization at a 90° angle to the domain boundary leads to a bound charge at the boundary, as shown in Eq 1 [212,213]:

$$\rho_{pol} = \nabla P \tag{1}$$

where, ρ_{pol} is the bound charge density. This bound charge gives rise to a depolarizing electric field in a reverse direction to the spontaneous polarization. The existence of strongly-ordered polarized domains in the perovskite gives rise to the formation of channels for minimizing charge recombinations and efficient charge transports in the device, which result in a high short-circuit current (JSC) and fill factor (FF). This important domain ordering is, nevertheless, doubtful to take place in actual devices. In the case of arbitrarily interrelated polarization in domains, a realistic scenario, it has been illustrated that holes and electrons emerge to pursue pathways or channels in the perovskite, leading to lower charge recombinations and efficient charge transports in the photovoltaic cell as proved by high FFs [213].

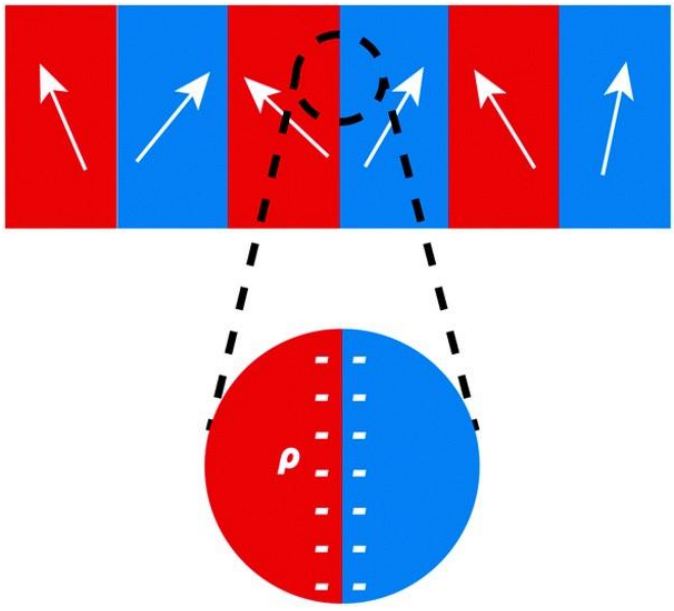

Figure 10. Spontaneous polarization induced domains in a ferroelectric material (Reproduced from Ref. [213] with permission).

The P_i ($C \cdot m^{-2}$) polarization is produced in dielectric and insulating materials with the application of the electric field vector E_i ($V \cdot m^{-1}$) (Eq 2):

$$P_i = \chi_{ij} E_j \tag{2}$$

where χ_{ij} ($F \cdot m^{-1}$) is the 2nd-rank tensor identified as the material's dielectric susceptibility. Eq 2 is valid only in a linear limit for nonlinear materials or for linear materials. Generally, the polarization, P_i, depends on higher-order terms of the field. Similarly, the total surface charge density induced in the material by applying the applied field is obtained using the dielectric displacement vector, D_i ($C \cdot m^{-2}$), shown in Eq 3:

$$D_i = \varepsilon_0 E_i C P_i \tag{3}$$

Scalar $\varepsilon_0 = 8.854 \times 10^{-12}$ $F \cdot m^{-1}$ and is called the dielectric permittivity of a vacuum. Thus, Eq 4 is obtained from Eqs 2 and 3, that:

$$D_i = \varepsilon_0 E_i + \chi_{ij} E_j = \varepsilon_0 \delta_{ij} E_j + \chi_{ij} E_j = (\varepsilon_0 \delta_{ij} + \chi_{ij}) Ej = \varepsilon_{ij} E_j \tag{4}$$

where δ_{ij} is Kronecker's symbol and $\varepsilon_{ij} = \varepsilon_0 \delta_{ij} + \chi_{ij}$ is the material's dielectric permittivity. $\delta_{ij} = 0$, for $i \neq j$; $\delta_{ij} = 1$ for $i = j$. In most ferroelectric materials, $\varepsilon_{ij} \neq \chi_{ij}$ and $\varepsilon_0 \delta_{ij} << \chi_{jj}$. In fact, the comparative dielectric permittivity, $k_{ij} = \varepsilon_{ij}/\varepsilon_0$, identified as a material dielectric constant is usually taken compared to the dielectric permittivity. Taking free energy opinion, it can simply be illustrated that χ_{ij} (also ε_{ij} and k_{ij}) have to be a symmetrical tensor ($\chi_{ij} = \chi_{ji}$) with only six autonomous mechanisms [214–216].

Like ferroelectrics, it would of great interest to deal with and understand piezoelectric properties and applications of halide perovskite materials. The word piezoelectrics is used to explain attractive properties of technological important classes of materials with a diversity of functionalities, ranging from ultrasound transducers, fuel injectors, and waveguide devices to gyroscopes and accelerometers [217–219]. It is of high technological interest to explore the piezoelectric properties of the hybrid perovskites for applications such as piezoelectric generators or energy harvesting devices [220,221]. In this section, origin of piezoelectrics, the sunrise of piezoelectrics, methods to enhance hybrid perovskite piezoelectrics, possibility of constructing dampers, and low loss piezoelectrics are issues that should not be missed while studying piezoelectrics. Other important points are also discussed.

The piezoelectric effect consists of strain development under the application of an electric field. Moreover, piezoelectricity is a basic procedure that includes multiple piezoelectric equations and diverse electromechanical effects. The direct piezoelectric effect relates to the produced polarization that builds up in i direction (ΔPi) with an applied stress in direction j (σ_j in Voigt notation) as in Eq 5 [222]:

$$\Delta P_i = d_{ij} \sigma_j \tag{5}$$

where, d_{ij} is 3rd-rank tensor, and every d_{ij} is typically called a piezoelectric coefficient or direct piezoelectric strain coefficient in units of pC/N. An additional piezoelectric equation between the polarization with the strain η is specified by Eq 6 [222]:

$$\Delta P_i = e_{ij} \eta_j \tag{6}$$

where the e_{ij} is the piezoelectric stress coefficient in the unit of C/m^2. It is indicated that the d_{ij} and e_{ij} parameters are associated with each other using stiffness and/or elastic compliances, though d_{ij} is simple to determine experimentally. The total generated polarization articulated in the c direction is given by Eq 7 [222]:

$$\Delta P_3 = e_{33}\eta_3 + e_{31}(\eta_1 + \eta_2) \tag{7}$$

where, Eqs 8 and 9 are obtained:

$$\eta_1 = \frac{(x-x_0)}{x_0} \tag{8}$$

$$\eta_2 = \frac{(y-y_0)}{y_0}$$

$$\eta_3 = \frac{(z-z_0)}{z_0} \tag{9}$$

are strains along the *x*, *y*, and *z* axis, with x_0, y_0, and z_0 as lattice constants for a structure not strained.

In order to disclose the source of piezoelectricity [223], it is important to split the total polarization originated from contributions of the (1) A-site MA cations and (2) B-site Pb atoms. The Pb atom induced polarization is measured using $D(Pb)/Vu \times P_{Pb} = Z_{33}$ [222], where Z_{33} is the Born effective charge of Pb, D(Pb) is the average displacement of Pb alongside the c axis with respect to the center of its I_6 cage, and Vu is the volume of the primitive unit cell. Thus, +4.24 is the measured value from the contribution of Z_{33}, which is considerably greater than the supposed charge of Pb (+2.0) in a pure ionic image [222] that implies the presence of a dynamic charge transfer coupled with the change of Pb–I bond length and the strong covalence of the Pb–I bonds. It is obvious that both molecular dipoles and Pb displacements are in charge of the total polarization in which Pb atoms contributes nearly all the piezoelectric response with negligible contribution from the MA^+ molecules.

In perovskites with unusual atomic substitutions in the ABX_3 architecture, the competition between B–X metal-halide bond and A–X hydrogen bond monitors the piezoelectric characteristics, drawing attention to the perspective of a halide perovskite design for manipulative and useful photopiezoelectrics and photoferroelectrics [222], such as applications in sensors, actuators, and energy harvesting [219,224–226]. Because of the pairing of semiconducting properties with its piezoelectrics, micro- and nanowires of piezoelectric semiconductors have been utilized as fundamental building blocks for developing ground-breaking devices [227], including piezo-phototronic devices [228,229], piezoelectric diodes [230], piezoelectric field-effect transistors [231], piezoelectric chemical sensors [232], and nanogenerators [233–235].

Thus, halide perovskites possess a cubic crystal structure that gives rise to ferroelectric polarizations similar to other classes of perovskites with identical structural characters [180,236–239]. Coll et al. have demonstrated the polarization switching and light-enhanced piezoelectricity of $CH_3NH_3PbI_3$ materials [240]. Furthermore, an output piezoelectric of 2.7 V and 140 $nA \cdot cm^{-2}$ have been reported [241], hindering the practical functionalities due to its modest output performance. Moreover, the highest piezoelectric current density and output voltage of 3.8 $\mu A \cdot cm^{-2}$ and 8.5 V have been demonstrated from the piezoelectric nanogenerator under periodically vertical compression.

Multilayered halide perovskites even have large polarization or strong piezoelectricity ≈1540 $p \cdot CN^{-1}$ [242]. This output is quite promising compared to other literature reports [243]. This could help charge LED and capacitors through a bridge rectifier.

8.8. Interface and defect engineering

In the field of halide double perovskites, the interfacial properties, especially those between the active perovskite layer and hole transporting layers, are not well touched. Recently, using Cu_2O as hole transporting material, a power conversion efficiency of 11.32% $Cs_2AgBiBr_6$ based solar cell was achieved, as indicated by the numerical simulations [244]. This indicates that the hole transport layer with a suitable alignment to the active layer makes an efficient charge transport process that can improve the challenges faced by Cs_2TiBr_6 and $Cs_2AgBiBr_6$. Furthermore, the grain boundary interfaces present in the active perovskite layer in addition to the other grain boundary interfaces present between various layers is a vital research lesson for improving the PEC and the performance. This is because considerable detrimental trap states in the electronic state of the valence and conduction band states of the halide double perovskite semiconductors might exist, which increases the carrier recombination rate and reduces the open circuit voltage significantly. Therefore, the engineering of the grain boundaries to eliminate the detrimental trap states in polycrystalline thin films becomes a long-standing and important issue for high performance optoelectronic devices [245–249]. In addition to the detrimental trap states, understanding the defect properties of the surface and bulk perovskite films, grain boundary, and surface passivation mechanisms, defect properties of the interface during engineering the device architecture is quite a crucial aspect that needs serious interface and defect engineering [245,246].

Moreover, Cs_2TiBr_6 is reported as a sensitive material to defect density [44,250,251] though it demonstrates a power conversion efficiency of 14.8% [252]. If all possible solar parameters are optimized, this solar material is a promising candidate for the future of peroveskite solar cells. Moreover, the numerical approach shows that a power conversion efficiency of 24.49% can be achieved by Cs_2PtI_6-based Cs_2TiBr_6 perovskite solar cells while Cs_2TiBr_6 is just 9.81% if it is well optimized [253]. Furthermore, the poor device performance of Cs_2TiBr_6 based peroveskite solar cells is because of the bulk defect present within the Cs_2TiBr_6 active light absorbing layer. Hence, defect passivation approaches are expected to solve defect related challenges in these materials. Thus, based on this defect optimization method, 9.9% efficiency has been achieved for Cs_2TiBr_6-based peroveskite solar cells [254]. Defects are also important to reconstruct band edges as shown in Figure 11. Such defects are intentionally incorporated defects useful to create new semiconducting materials [245]. The dominant metal orbital character of the bands is shown in color. Arrows show the direct (Figure 11a,b, $(MA)_2TlBiBr_6$) and indirect (Figure 11c, $Cs_2AgBiBr_6$) band gap transitions. In the primitive unit cell of 1 the VBM appears at X, however, in the conventional setting shown in Figure 11 the VBM is at Γ owing to band folding.

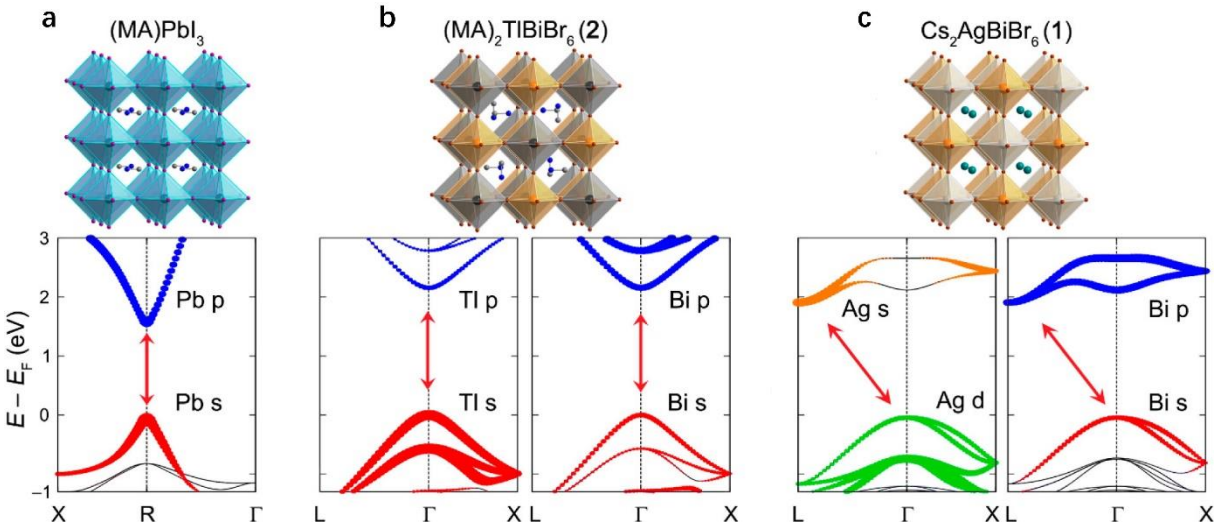

Figure 11. Crystal structures and band structures of (a) cubic $(MA)PbI_3$, (b) $(MA)_2TlBiBr_6$ and (c) $Cs_2AgBiBr_6$ (Reproduced from Ref. [245] with permission).

8.9. Device architectural engineering

Engineering the light harvesting active halide double peroveskite layer and interface between the active layer and different charge transporting layers as well as between the transporting layers and the charge collecting electrodes are indispensable prerequisites for appreciable performance. However, engineering the materials and the interface among various layers is not adequate. This is because the closing stages are eventually paying attention to the device performance for a specific application. As a result, engineering appropriate device architecture [255–257] is mandatory.

8.10. Doping engineering

Halide double perovskites become less suitable solutions to replace the unstable organic-inorganic halide perovskite solar cells. This is due to their indirect or direct as well as larger band gaps [18,40,147]. Therefore, doping engineering [18,200] is another strategy to achieve a band gap, which is suitable for light harvesting applications [23,185,258–260] This along with a chemical substitution approach might be done in all lattice sites of the double perovskite ($A_2(B^+, B^{3+})X_6$) available for substitution [23,185,258]. In this case, the degrees of freedom, with over 34 choices of trivalent metals available for selection, are mostly provided from the B^{3+} lattice site [259–261].

8.11. Equilibrium and non-equilibrium quantum transport

These transport properties and the effect of the spin-orbit on these properties is unclear: Studies on these properties could shed light to provide insightful understanding on why inferior device performances of halide double perovskites solar cells are happening.

9. Conclusions

$A_2B^IB^{III}X_6$ based lead-free halide double perovskite solar cells have been reported as promising nontoxic and stable candidates to replace organic-inorganic halide perovskite solar cells. Thus, such lead-free halide double perovskites have a (1) diversity of various families, (2) diversity of structural, optical and electrical properties, and (3) wide range of energy applications. Furthermore, the key origins of these diversities and variations are: cation displacement, cation anion ordering, ordered vacancies, tuneability of structural dimension, octahedral distortions, and tilting from the ideal structure. In addition, polarization, molecular dipoles, and tilting on the band structure are key origins of optoelectronic properties in halide double perovskites. Although lead-free halide double perovskite solar cells have promising opportunities such as a relatively longer photoluminescence lifetime and higher stability towards moisture, temperature, and light compared to lead halide perovskites, these solar cell devices have bottleneck challenges at material, interface, and device levels. Such challenges include: (a) inferior material and device power conversion efficiency, which is 2.5% using $Cs_2AgBiBr_6$ and 3.3% using Cs_2TiBr_6; (b) limited integration with interfacial materials; (c) quantum confinement effect of interacting orbitals of adjacent cations, which might result in broader band gaps and localized conduction bands; (d) high processing temperature, which may limit the diverse applications; and (e) low electronic dimensionality, making them less appropriate for single junction solar cell functions. Thus, it is suggested that material surfaces and bulk engineering, device architectural engineering, interfacial engineering, composition engineering, band gap engineering, doping engineering, polar and domain order engineering, etc., may be possible mechanisms to overcome the challenges. In addition, promising candidate characteristics, for instance, long charge carrier diffusion lengths, defect tolerance, low exciton binding energies, small carrier effective masses, intrinsic thermodynamic stability, direct band gaps, high absorption coefficient, and compatibility with low-cost and solution-supported fabrication procedures are highlighted for further considerations. This review will serve as a research roadmap for performance improvement for the lead and tin free halide double perovskite solar cell scientific community, research institutions, and commercial enterprises. Moreover, the challenge in most solar cells is the issue of sustainability.

With this in mind, the sustainability issue of $A_2B^IB^{III}X_6$ such as $Cs_2AgBiBr_6$ and Cs_2TiBr_6 perovskite solar cells shall be analyzed not only in terms of the balance among environment, equity, economy, affordability, energy independence, availability of desirable materials, and conditions over the long term but also the quality of being able to continue over a period of time. Thus, the researchers have to work in a way that they can confirm the sustainability issue of $A_2B^IB^{III}X_6$ based perovskite solar cells.

Use of AI tools declaration

The authors declare they have not used Artificial Intelligence (AI) tools in the creation of this article.

Author contributions

The first author, Etsana Kiros Ashebir, is responsible for manuscript writing, literature review, and the conceptualization, while Berhe Tadesse Abay is participated as a co-member of the project, bringing in expertise in materials properties and assisting with data analysis. Taame Abraha Berhe is main advisor of the research project, providing guidance and expertise in the field of halide double perovskite solar cell as well as serving the corresponding author of the idea and content designer. All authors have read and approved the final manuscript.

Conflicts of interest

The authors declare no conflict of interest.

Reference

1. Xing GH, Mathews N, Lim SS, et al. (2014) Low-temperature solution-processed wavelength-tunable perovskites for lasing. *Nature Mater* 13: 476–480. https://doi.org/10.1038/nmat3911
2. Tan ZK, Moghaddam RS, Lai ML, et al. (2014) Bright light-emitting diodes based on organometal halide perovskite. *Nature Nanotech* 9: 687–692. https://doi.org/10.1038/nnano.2014.149
3. Chin XY, Cortecchia D, Yin J, et al. (2015) Lead iodide perovskite light-emitting field-effect transistor. *Nat Commun* 6: 7383. https://doi.org/10.1038/ncomms8383
4. Boix PP, Nonomura K, Mathews N, et al. (2014) Current progress and future perspectives for organic/inorganic perovskite solar cells. *Mater Today* 17: 16–23. https://doi.org/10.1016/j.mattod.2013.12.002
5. Zhao XG, Yang DW, Ren JC, et al. (2018) Rational design of halide double perovskites for optoelectronic applications. *Joule* 2: 1662–1673. https://doi.org/10.1016/j.joule.2018.06.017
6. Li ZZ, Yin WJ (2018) Recent progress in Pb-free stable inorganic double halide perovskites. *J Semicond* 39: 071003. https://dx.doi.org/10.1088/1674-4926/39/7/071003
7. Kumar MH, Dharani S, Leong WL, et al. (2014) Lead-free halide perovskite solar cells with high photocurrents realized through vacancy modulation. *Adv Mater* 26: 7122–7127. https://doi.org/10.1002/adma.201401991
8. Hao F, Stoumpos CC, Cao DH, et al. (2014) Lead-free solid-state organic–inorganic halide perovskite solar cells. *Nat Photon* 8: 489–494. https://doi.org/10.1038/nphoton.2014.82
9. Harikesh PC, Mulmudi HK, Ghosh B, et al. (2016) Rb as an alternative cation for templating inorganic lead-free perovskites for solution processed photovoltaics. *Chem Mater* 28: 7496–7504. https://doi.org/10.1021/acs.chemmater.6b03310
10. Linaburg ETM, Matthew R, Majher Jackson D, et al. (2017) $Cs_{1-x}Rb_xPbCl_3$ and $Cs_{1-x}Rb_xPbBr_3$ solid solutions: Understanding octahedral tilting in lead halide perovskites. *Chem Mater* 29: 3507−3514. https://doi.org/10.1021/acs.chemmater.6b05372

11. Volonakis G, Haghighirad AA, Milot RL (2017) $Cs_2InAgCl_6$: A new lead-free halide double perovskite with direct band gap. *J Phys Chem Lett* 8: 772–778. https://doi.org/10.1021/acs.jpclett.6b02682
12. Zhao XG, Yang DW, Sun YH, et al. (2017) Cu-In halide perovskite solar absorbers. *J Am Chem Soc* 139: 6718–6725. https://doi.org/10.1021/jacs.7b02120
13. Ju MG, Chen M, Zhou YY, et al. (2018) Earth-abundant nontoxic titanium (IV)-based vacancy-ordered double perovskite halides with tunable 1.0 to 1.8 eV bandgaps for photovoltaic applications. *ACS Energy Lett* 3: 297−304. https://doi.org/10.1021/acsenergylett.7b01167
14. Pazoki M, Johansson MB, Zhu HM, et al. (2016) Bismuth iodide perovskite materials for solar cell applications: Electronic structure, optical transitions, and directional charge transport. *J Phys Chem C* 120: 29039−29046. https://doi.org/10.1021/acs.jpcc.6b11745
15. Hutter EM, Gelvez-Rueda MC, Bartesaghi D, et al. (2018) Band-like charge transport in $Cs_2AgBiBr_6$ and mixed antimony−bismuth $Cs_2AgBi_{1-x}Sb_xBr_6$ halide double perovskites. *ACS Omega* 3: 11655−11662. https://doi.org/10.1021/acsomega.8b01705
16. Gray MB, McClure ET, Woodward PM (2019) $Cs_2AgBiBr_{6-x}Cl_x$ solid solutions–band gap engineering with halide double perovskites. *J Mater Chem C* 7: 9686−9689. https://doi.org/10.1039/C9TC02674F
17. Hong KH, Kim J, Debbichi L, et al. (2017) Band gap engineering of $Cs_3Bi_2I_9$ perovskites with trivalent atoms using a dual metal cation. *J Phys Chem C* 121: 969−974. https://doi.org/10.1021/acs.jpcc.6b12426
18. Karmakar A, Dodd MS, Agnihotri S, et al. (2018) Cu(II)-doped $Cs_2SbAgCl_6$ double perovskite: A lead-free, low-bandgap material. *Chem Mate*r 30: 8280−8290. https://doi.org/10.1021/acs.chemmater.8b03755
19. Zhou J, Xia Z, Molokeev MS, et al. (2017) Composition design, optical gap and stability investigations of lead-free halide double perovskite Cs_2AgInC_{l6}. *J Mater Chem A* 5: 15031−15037. https://doi.org/10.1039/C7TA04690A
20. Chu L, Ahmad W, Liu W, et al (2019) Lead-free halide double perovskite materials: A new superstar toward green and stable optoelectronic applications. *Nanomicro Lett* 11: 16. https://doi.org/10.1007/s40820-019-0244-6
21. Tang Y, Liang M, Chang B, et al. (2019) Lead-free double halide perovskite Cs_3BiBr_6 with well-defined crystal structure and high thermal stability for optoelectronics. *J Mater Chem C* 7: 3369−3374. https://doi.org/10.1039/C8TC05480K
22. Luo J, Wang X, Li S, et al. (2018) Efficient and stable emission of warm-white light from lead-free halide double perovskites. *Nature* 563: 541−545. https://doi.org/10.1038/s41586-018-0691-0
23. Filip MR, Liu X, Miglio A, et al. (2018) Phase diagrams and stability of lead-free halide double perovskites $Cs_2BB'X_6$: B = Sb and Bi, B′ = Cu, Ag, and Au, and X = Cl, Br, and I. *J Phys Chem C* 122: 158−170. https://doi.org/10.1021/acs.jpcc.7b10370
24. Flerova IN, Goreva MV, Aleksandrova KS, et al. (1998) Phase transitions in elpasolites (ordered perovskites). *Mater Sci Eng R* 24: 81−151. https://doi.org/10.1016/S0927-796X(98)00015-1
25. Morss LR, Siegal M, Stenger L, et al. (1970) Preparation of cubic chloro complex compounds of trivalent metals: Cs_2NaMCl_6. *Inorg Chem* 9: 1771−1775. https://doi.org/10.1021/ic50089a034

26. Khalfin S, Bekenstein Y (2019) Advances in lead-free double perovskite nanocrystals, engineering band-gaps and enhancing stability through composition tunabilty. *Nanoscale* 11: 8665−8679. https://doi.org/10.1039/C9NR01031A
27. Igbari F, Wang ZK, Liao LS (2019) Progress of lead-free halide double perovskites. *Adv Energy Mater* 9: 1803150. https://doi.org/10.1002/aenm.201803150
28. Meyer E, Mutukwa D, Zingwe N, et al. (2018) Lead-free halide double perovskites: A review of the structural, optical, and stability properties as well as their viability to replace lead halide perovskites. *Metals* 8: 667. https://doi.org/10.3390/met8090667
29. Slavney AH, Leppert L, Valdes AS, et al. (2018) Small-bandgap halide double perovskites. *Angew Chem Int Ed* 57: 12765 https://doi.org/10.1002/anie.201807421
30. NREL Efficiency Chart. This Plot Is Courtesy of the National Renewable Energy Laboratory, Golden, CO. Available from: https://www.nrel.gov/pv/assets/pdfs/best-reserch-cell-efficiencies..20190411.pdf (accessed on 14 April 2019).
31. Chen B, Yu Z, Liu K, et al. (2019) Grain engineering for perovskite/silicon monolithic tandem solar cells with efficiency of 25.4%. *Joule* 3: 177−190. https://doi.org/10.1016/j.joule.2018.10.003
32. Al-Ashouri A, Köhnen E, Li B, et al. (2020) Monolithic perovskite/silicon tandem solar cell with 29% efficiency by enhanced hole extraction. *Science* 370: 1300−1309. https://doi.org/10.1126/science.abd401
33. Chen M, Ju MG, Garces HF, et al. (2019) Highly stable and efficient all-inorganic lead-free perovskite solar cells with native-oxide passivation. *Nat Commun* 10: 16. https://doi.org/10.1038/s41467-018-07951-y
34. Nalianya MA, Awino C, Barasa H, et al. (2021) Numerical study of lead free $CsSn_{0.5}Ge_{0.5}I_3$ perovskite solar cell by SCAPS-1D. *Optik* 248: 168060. https://doi.org/10.1016/j.ijleo.2021.168060
35. Liu X, Li T, Hao L, et al. (2023) Lead free $CsSn_{0.5}Ge_{0.5}I_3$ perovskite solar cell with different layer properties via SCAPS-1D simulation. *CJCE* 101: 6792−6806. https://doi.org/10.1002/cjce.25009
36. Singh NK, Agarwal A (2023) Performance assessment of sustainable highly efficient $CsSn_{0.5}Ge_{0.5}I_3$/$FASnI_3$ based perovskite solar cell: A numerical modelling approach. *Opt Mater* 139: 113822. https://doi.org/10.1016/j.optmat.2023.113822
37. Aktas E, Rajamanickam N, Pascual J, et al. (2022) Challenges and strategies toward long-term stability of lead-free tin-based perovskite solar cells. *Commun Mater* 3: 104. https://doi.org/10.1038/s43246-022-00327-2
38. Saparov B, Sun JP, Meng W, et al. (2016) Thin film deposition and characterization of a Sn-deficient perovskite derivative Cs_2SnI_6. *Chem Mater* 28: 2315–2322. https://doi.org/10.1021/acs.chemmater.6b00433
39. López-Fernández I, Valli D, Wang CY, et al. (2024) Lead-free halide perovskite materials and optoelectronic devices: Progress and prospective. *Adv Funct Mater* 34: 2307896. https://doi.org/10.1002/adfm.202307896

40. Greul E, Petrus ML, Binek A, et al. (2017) Highly stable, phase pure $Cs_2AgBiBr_6$ double perovskite thin films for optoelectronic applications. *J Mater Chem A* 5: 19972–19981. https://doi.org/10.1039/C7TA06816F
41. Yang X, Chen Y, Liu P, et al. (2020) Simultaneous power conversion efficiency and stability enhancement of $Cs_2AgBiBr_6$ lead-free inorganic perovskite solar cell through adopting a multifunctional dye interlayer. *Adv Funct Mater* 30: 2001557. https://doi.org/10.1002/adfm.202001557
42. Zhang Z, Sun Q, Lu Y, et al. (2022) Hydrogenated $Cs_2AgBiBr_6$ for significantly improved efficiency of lead-free inorganic double perovskite solar cell. *Nat Commun* 13: 3397. https://doi.org/10.1038/s41467-022-31016-w
43. Chen M, Ju MG, Carl AD, et al. (2018) Cesium titanium(IV) bromide thin films based stable lead-free perovskite solar cells. *Joule* 2: 1–13. https://doi.org/10.1016/j.joule.2018.01.009
44. Ahmed S, Jannat F, Khan MAK, et al. (2021) Numerical development of eco-friendly Cs_2TiBr_6 based perovskite solar cell with all-inorganic charge transport materials via SCAPS-1D. *Optik* 225: 165765. https://doi.org/10.1016/j.ijleo.2020.165765
45. Mercy PAM, Wilson KSJ (2023) Development of environmental friendly high performance Cs_2TiBr_6 based perovskite solar cell using numerical simulation. *Appl Surf Sci Adv* 15: 100394. https://doi.org/10.1016/j.apsadv.2023.100394
46. Zhang P, Yang J, Wei SH (2018) Manipulation of cation combinations and configurations of halide double perovskites for solar cell absorbers. *J Mater Chem A* 6: 1809–1815. https://doi.org/10.1039/C7TA09713A
47. Berhe TA, Su WN, Chen CH, et al. (2016) Organometal halide perovskite solar cells: Degradation and stability. *Energy Environ Sci* 9: 323–356. https://doi.org/10.1039/C5EE02733K
48. Dai X, Deng Y, Van BCH, et al. (2019) Meniscus fabrication of halide perovskite thin films at high throughput for large area and low-cost solar panels. *IJEM* 1: 022004. https://doi.org/10.1088/2631-7990/ab263e
49. Tiing TV (2018) Octadecylamine-functionalized single-walled carbon nanotubes for facilitating the formation of a monolithic perovskite layer and stable solar cells. *Adv Funct Mater* 28: 1705545. https://doi.org/10.1002/adfm.201705545
50. Wu S, Liu Y (2023) Recent advancements and manipulation strategies of colloidal $Cs_2BIBIIIX_6$ lead-free halide double perovskite nanocrystals. *Nano Res* 16: 5572–5591. https://doi.org/10.1007/s12274-022-5232-3
51. Volonakis GF, Haghighirad MR, Sakai AA, et al. (2016) Lead-free halide double perovskites via heterovalent substitution of noble metals. *J Phys Chem Lett* 7: 1254−1259. https://doi.org/10.1021/acs.jpclett.6b00376
52. Roknuzzaman M, Zhang C, Ostrikov K, et al. (2019) Electronic and optical properties of lead-free hybrid double perovskites for photovoltaic and optoelectronic applications. *Sci Rep* 9: 718. https://doi.org/10.1038/s41598-018-37132-2
53. Stoumpos CC, Malliakas CD, Kanatzidis MG, et al. (2013) Semiconducting tin and lead iodide perovskites with organic cations: Phase transitions, high mobilities and near-infrared photoluminescent properties. *Inorg Chem* 52: 9019–9038. https://doi.org/10.1021/ic401215x

54. Ponseca CS, Savenije TJ, Abdellah M, et al. (2014) Organometal halide perovskite solar cell materials rationalized: Ultrafast charge generation, high and microsecond-long balanced mobilities, and slow recombination. *J Am Chem Soc* 136: 5189–5192. https://doi.org/10.1021/ja412583t
55. Pham HQ, Holmes RJ, Aydil ES, et al. (2019) Lead-free double perovskites $Cs_2InCuCl_6$ and $(CH_3NH_3)_2InCuCl_6$: Electronic, optical and electrical properties. *Nanoscale* 11: 11173–11182. https://doi.org/10.1039/C9NR01645G
56. Wei F, Deng Z, Sun S (2017) Synthesis and properties of a lead-free hybrid double perovskite: $(CH_3NH_3)_2AgBiBr_6$. *Chem Mater* 29: 1089–1094. https://doi.org/10.1021/acs.chemmater.6b03944
57. Xing G, Mathews N, Sun S, et al. (2013) Long-range balanced electron- and hole-transport lengths in organic-inorganic $CH_3NH_3PbI_3$. *Science* 342: 344–347. https://doi.org/10.1126/science.124316
58. Etgar L, Gao P, Xue Z, et al. (2012) Mesoscopic $CH_3NH_3PbI_3/TiO_2$ heterojunction solar cells. *J Am Chem Soc* 134: 17396–17399. https://doi.org/10.1021/ja307789s
59. Ball JM, Lee MM, Hey A, et al. (2013) Low-temperature processed meso-superstructured to thin-film perovskite solar cells. *Energy Environ Sci* 6: 1739–1743. https://doi.org/10.1039/C3EE40810H
60. Jeon NJ, Noh JH, Kim YC, et al. (2014) Solvent engineering for high-performance inorganic–organic hybrid perovskite solar cells. *Nat Mater* 13: 897–903. https://doi.org/10.1038/nmat4014
61. Burschka J, Pellet N, Moon SJ, et al. (2013) Sequential deposition as a route to high-performance perovskite-sensitized solar cells. *Nature* 499: 316–319. https://doi.org/10.1038/nature12340
62. Liu D, Kelly TL (2014) Perovskite solar cells with a planar heterojunction structure prepared using room-temperature solution processing techniques. *Nat Photon* 8: 133–138. https://doi.org/10.1038/nphoton.2013.342
63. Eperon GE, Stranks SD, Menelaou C (2014) Formamidinium lead trihalide: A broadly tunable perovskite for efficient planar heterojunction solar cells. *Energy Environ Sci* 7: 982–988. https://doi.org/10.1039/C3EE43822H
64. Kojima A, Teshima K, Shirai Y, et al. (2009) Organometal halide perovskites as visible-light sensitizers for photovoltaic cells. *J Am Chem Soc* 131: 6050–6051. https://doi.org/10.1021/ja809598r
65. Ghanshyam PVB, Kim C, Lookman T (2016) Finding new perovskite halides via machine learning. *Front Mater* 3: 19. https://doi.org/10.3389/fmats.2016.00019
66. Gonzalez-Pedro V, Juarez-Perez EJ, Arsyad WS (2014) General working principles of $CH_3NH_3PbX_3$ perovskite solar cells. *Nano Lett* 14: 888–893. https://doi.org/10.1021/nl404252e
67. Uddin MA, Calabro RL, Kim DY, et al. (2018) Halide exchange and surface modification of metal halide perovskite nanocrystals with alkyltrichlorosilanes. *Nanoscale* 10: 16919–16927. https://doi.org/10.1039/C8NR04763D
68. Protesescu L, Yakunin S, Bodnarchuk MI (2015) Nanocrystals of cesium lead halide perovskites ($CsPbX_3$, X = Cl, Br, and I): Novel optoelectronic materials showing bright emission with wide color gamut. *Nano Lett* 15: 3692–3696. https://doi.org/10.1021/nl5048779

69. Nedelcu G, Protesescu L, Yakunin S (2015) Fast anion-exchange in highly luminescent nanocrystals of cesium lead halide perovskites ($CsPbX_3$, X = Cl, Br, I). *Nano Lett* 15: 5635–5640. https://doi.org/10.1021/acs.nanolett.5b02404
70. Jeon JHN, Yang WS, Kim YC, et al. (2015) Compositional engineering of perovskite materials for high-performance solar cells. *Nature* 517: 476–480. https://doi.org/10.1038/nature14133
71. Lee JW, Kim DH, Kim KS, et al. (2015) Formamidinium and cesium hybridization for photo- and moisture-stable perovskite solar cell. *Adv Energy Mater* 5: 1501310. https://doi.org/10.1002/aenm.201501310
72. Park YH, Jeong I, Bae S, et al. (2017) Inorganic rubidium cation as an enhancer for photovoltaic performance and moisture stability of $HC(NH_2)_2PbI_3$ perovskite solar cells. *Adv Funct Mater* 27: 1605988. https://doi.org/10.1002/adfm.201605988
73. Locardi F, Cirignano M, Dmitry BZD, et al. (2018) Colloidal synthesis of double perovskite $Cs_2AgInCl_6$ and Mn-doped $Cs_2AgInCl_6$ nanocrystals. *J Am Chem Soc* 140: 12989–12995 https://doi.org/10.1021/jacs.8b07983
74. Stoumpos CCF, Clark L, Kim DJ, et al. (2015) Hybrid germanium iodide perovskite semiconductors: Active lone pairs, structural distortions, direct and indirect energy gaps, and strong nonlinear optical properties. *J Am Chem Soc* 137: 6804−6819. https://doi.org/10.1021/jacs.5b01025
75. Berhe TA, Su WN, Hwang BJ (2024) Halide perovskites' multifunctional properties: Coordination engineering, coordination chemistry, electronic interactions and energy applications beyond photovoltaics. *Inorganics* 12: 182. https://doi.org/10.3390/inorganics12070182
76. Hua WAE, Johansson MB, Wang J, (2021) Mixed-halide double perovskite Cs_2AgBiX_6 (X = Br, I) with tunable optical properties via anion exchange. *ChemSusChem* 14: 4507–4515. https://doi.org/10.1002/cssc.202101146
77. Abdulmutta T, Rassamessan A (2024) First-principles study on structural, electronic and optical properties of mixed alloys of $Cs_2Ag(Sb_xBi)$. *Comput Mater Sci* 239. https://doi.org/10.1039/D3RA02566G
78. Noel NK, Stranks SD, Abate A, et al. (2014). Lead-free organic–inorganic tin halide perovskites for photovoltaic applications. *Energy Environ Sci* 7: 3061–3068. https://doi.org/10.1039/C4EE01076K
79. Xiao ZY, Shao Y, Wang Y, et al. (2015) Giant switchable photovoltaic effect in organometal trihalide perovskite devices. *Nat Mater* 14: 193−198. https://doi.org/10.1038/nmat4150
80. Bertoluzzi LS, Liu RS, Lee L, et.al. (2015) Cooperative kinetics of depolarization in $CH_3NH_3PbI_3$ perovskite solar cells. *Energy Environ Sci* 8: 910–915. https://doi.org/10.1039/C4EE03171G
81. Snaith HJA, Ball A, Eperon JM, et al. (2014) Anomalous hysteresis in perovskite solar cells. *J Phys Chem Lett* 5: 1511–1515. https://doi.org/10.1021/jz500113x
82. Tress WM, Moehl N, Zakeeruddin T, et al. (2015) Understanding the rate-dependent J-V hysteresis, slow time component, and aging in $CH_3NH_3PBI_3$ perovskite solar cells: The role of a compensated electric field. *Energy Environ Sci* 8: 995–1004. https://doi.org/10.1039/C4EE03664F

83. Hoke ET, Slotcavage DJ, Dohner ER, et al. (2015) Reversible photo-induced trap formation in mixed-halide hybrid perovskites for photovoltaics. *Chem Sci* 6: 613–617. https://doi.org/10.1039/C4SC03141E
84. Fan ZX, Sun J, Chen K, et al. (2015) Ferroelectricity of $CH_3NH_3PbI_3$ perovskite. *J Phys Chem Lett* 6: 1155–1161. https://doi.org/10.1021/acs.jpclett.5b00389
85. Rong Y, Hu Y, Ravishankar S, et al. (2017) Tunable hysteresis effect for perovskite solar cells, *Energy Environ Sci* 10: 2383–2391. https://doi.org/10.1039/C7EE02048A
86. Balaguera EH, Bisquert J (2024) Accelerating the assessment of hysteresis in perovskite solar cells. *ACS Energy Lett* 9: 478–486. https://doi.org/10.1021/acsenergylett.3c02779
87. Singh R, Parashar M (2020) Origin of hysteresis in perovskite solar cells, In: Ren JZ, Kan ZP, *Soft-Matter Thin Film Solar Cells: Physical Processes and Device Simulation*, New York: AIP Publishing LLC. https://doi.org/10.1063/9780735422414_001
88. Kim HS, Park NG (2014) Parameters affecting I–V hysteresis of $CH_3NH_3PbI_3$ perovskite solar cells: Effects of perovskite crystal size and mesoporous TiO_2 layer. *J Phys Chem Lett* 5: 2927–2934. https://doi.org/10.1021/jz501392m
89. Leijtens T, Ram SKA, Eperon GE, et al. (2015) Modulating the electron-hole interaction in a hybrid lead halide perovskite with an electric field. *J Am Chem Soc* 137: 15451–15459. https://doi.org/10.1021/jacs.5b09085
90. Chaves A, Azadani JG, Alsalman H, et al. (2020) Low bandgap engineering of two-dimensional semiconductor materials. *npj 2D Mater Appl* 4: 29. https://doi.org/10.1038/s41699-020-00162-4
91. Prasanna R, Gold-Parker A, Leijtens T, et al. (2017) Band gap tuning via lattice contraction and octahedral tilting in perovskite materials for photovoltaics. *J Am Chem Soc* 139: 11117–11124. https://doi.org/10.1021/jacs.7b04981
92. Lee JH, Bristowe NC, Lee JH, et al. (2016) Resolving the physical origin of octahedral tilting in halide perovskites. *Chem Mater* 28: 4259–4266. https://doi.org/10.1021/acs.chemmater.6b00968
93. Bechtel JS, Van der Ven A (2018) Octahedral tilting instabilities in inorganic halide perovskites. *Phys Rev Materials* 2: 025401. https://doi.org/10.1103/PhysRevMaterials.2.025401
94. Yang RX, Skelton JM, Silva EL, et al. (2017) Spontaneous octahedral tilting in the cubic inorganic cesium halide perovskites $CsSnX_3$ and $CsPbX_3$ (X = F, Cl, Br, I). *J Phys Chem Lett* 8: 4720−4726. https://doi.org/10.1021/acs.jpclett.7b02423
95. Shao Y, Gao W, Yan H, (2022) Unlocking surface octahedral tilt in twodimensional Ruddlesden-Popper perovskites. *Nat Commun* 13: 138. https://doi.org/10.1038/s41467-021-27747-x
96. Klarbring J (2018) Low energy paths for octahedral tilting in inorganic halide perovskites. *Phys Rev B* 99: 104105. https://doi.org/10.1103/PhysRevB.99.104105
97. Munson KT, Kennehan ER, Doucette GS, et al. (2018) Dynamic disorder dominates delocalization, transport, and recombination in halide perovskites. *Chem* 4: 2826−2843. https://doi.org/10.1016/j.chempr.2018.09.00199
98. Lei H, Hardy D, Gao F (2021) Lead-free double perovskite $Cs_2AgBiBr_6$: Fundamentals, applications and perspectives. *Adv Funct Mater* 31: 2105898. https://doi.org/10.1002/adfm.202105898

99. Karunadasa HI, Slavney AH (2022) Alloyed halide double perovskites as solar-cell absorbers. Available from: https://www.osti.gov/servlets/purl/1892693.
100. Palmstrom AF, Eperon GE, Leijtens T, et al. (2019) Enabling flexible all-perovskite tandem solar cells. *Joule* 3: 1–12. https://doi.org/10.1016/j.joule.2019.05.009
101. Zhou L, Xu YF, Chen BX, et al. (2018) Synthesis and photocatalytic application of stable lead free $Cs_2AgBiBr_6$ perovskite nanocrystals. *Small* 14: 1703762. https://doi.org/10.1002/smll.201703762
102. Zhang ZZ, Liang Y, Huang H, et al. (2019) Stable and highly efficient photocatalysis with lead-free double-perovskite of $Cs_2AgBiBr_6$. *Angew Chem Int Ed* 58: 7263–7267. https://doi.org/10.1002/anie.201900658
103. Cho J, DuBose JT, Kamat PV (2020) Charge injection from excited $Cs_2AgBiBr_6$ quantum dots into semiconductor oxides. *Chem Mater* 32: 510–517. https://doi.org/10.1021/acs.chemmater.9b04243
104. Ippili S, Kim JH, Jella V, et al. (2023) Halide double perovskite-based efficient mechanical energy harvester and storage devices for self-charging power unit. *Nano Energy* 107: 108148. https://doi.org/10.1016/j.nanoen.2022.108148
105. Wu H, Pi J, Liu Q, et al. (2021) All-inorganic lead free double perovskite li-battery anode material hosting high Li^+ ion concentrations. *J Phys Chem Lett* 12: 4125–4129. https://doi.org/10.1021/acs.jpclett.1c00041
106. Zhang L, Miao J, Li J, et al. (2020) Halide perovskite materials for energy storage applications. *Adv Funct Mater* 30: 2003653. https://doi.org/10.1002/adfm.202003653
107. Yang S, Liang Q, Wu H, et al. (2022) Lead-free double perovskite $Cs_2NaErCl_6$: Li^+ as high-stability anodes for Li-ion batteries. *J Phys Chem Lett* 13: 4981–4987. https://doi.org/10.1021/acs.jpclett.2c01052
108. Choon SL, Lim HN (2024) Impact of vacancies in halide perovskites for batteries and supercapacitors. *Mater Today Energy* 43: 101577. https://doi.org/10.1016/j.mtener.2024.101577
109. Yadav A, Saini A, Kumar P, et al. (2024) Lead-free halide perovskites for high-performance thin-film flexible supercapacitor applications. *J Mater Chem C* 12: 197–206. https://doi.org/10.1039/D3TC02784H
110. Tan Y, Mu G, Chen M, et al. (2023) X-ray detectors based on halide perovskite materials. *Coatings* 13: 211. https://doi.org/10.3390/coatings13010211
111. Tailor NK, Ghosh J, Afroz MA, et al. (2022) Self-powered X-ray detection and imaging using $Cs_2AgBiCl_6$ lead-free double perovskite single crystal. *ACS Appl Electron Mater* 4: 4530–4539. https://doi.org/10.1021/acsaelm.2c00752
112. Li Z, Zhou F, Yao H, et al. (2021) Halide perovskites for high-performance X-ray detector. *Materials Today* 48: 155–175. https://doi.org/10.1016/j.mattod.2021.01.028
113. Saparov B, Mitzi DB (2016) Organic–inorganic perovskites: structural versatility for functional materials design. *Chem Rev* 116: 4558–4596. https://doi.org/10.1021/acs.chemrev.5b00715
114. Best Research-Cell Efficiency Chart. (2019) Available from: https://www.nrel.gov/pv/cell-efficiency.html.

115. Bhojak V, Bhatia D, Jain PK (2022) Investigation of photocurrent efficiency of Cs_2TiBr_6 double perovskite solar cell. *Mater Today Proc* 66: 3692–3697. https://doi.org/10.1016/j.matpr.2022.07.443
116. Qin X, Zhao Z, Wang Y, et al. (2017) Recent progress in stability of perovskite solar cells. *J Semicond* 38: 011002. https://doi.org/10.1088/1674-4926/38/1/011002
117. Berhe TA, Cheng JH, Su WN, et al. (2017) Identification of the physical origin behind disorder, heterogeneity, and reconstruction and their correlation with the photoluminescence lifetime in hybrid perovskite thin films. *J Mater Chem A* 5: 21002–21015. https://doi.org/10.1039/C7TA04615D
118. Xiao Z, Meng W, Wang J, et al. (2017) Searching for promising new perovskite-based photovoltaic absorbers: The importance of electronic dimensionality. *Mater Horiz* 4: 206–216. https://doi.org/10.1039/C6MH00519E
119. Zhang Q, Ting H, Wei S, et al. (2018) Recent progress in lead-free perovskite (-like) solar cells. *Mater Today Energy* 8: 157–165. https://doi.org/10.1016/j.mtener.2018.03.001
120. Kanno S, Imamura Y, Hada M (2019) Alternative materials for perovskite solar cells from materials informatics. *Phys Rev Mater* 3: 075403. https://doi.org/10.1103/PhysRevMaterials.3.075403
121. Liang L, Gao P (2018) Lead-free hybrid perovskite absorbers for viable application: Can we eat the cake and have it too? *Adv Sci (Weinh)* 5: 1700331. https://doi.org/10.1002/advs.201700331
122. Abate A (2017) Perovskite solar cells go lead free. *Joule* 1: 659–664. https://doi.org/10.1016/j.joule.2017.09.007
123. Xu Q, Yang D, Lv J, et al. (2018) Perovskite solar absorbers: Materials by design. *Small Methods* 2: 1700316. https://doi.org/10.1002/smtd.201700316
124. Volonakis G, Giustino F (2018) Surface properties of lead-free halide double perovskites: Possible visible-light photo-catalysts for water splitting featured. *Appl Phys Lett* 112: 243901. https://doi.org/10.1063/1.5035274
125. Slavney AH, Hu T, Lindenberg AM, et al. (2016) A bismuth-halide double perovskite with long carrier recombination lifetime for photovoltaic applications. *J Am Chem Soc* 138: 2138−2141. https://doi.org/10.1021/jacs.5b13294
126. Karunadasa HI, Slavney AH (2017) Halide double perovskite $Cs_2AgBiBr_6$ solar-cell absorber having long carrier lifetimes.
127. Savory CN, Walsh A, Scanlon DO (2016) Can Pb-free halide double perovskites support high-efficiency solar cells? *ACS Energy Lett* 1: 949−955. https://doi.org/10.1021/acsenergylett.6b00471
128. Pecunia V, Occhipinti LG, Chakraborty A (2020) Lead-free halide perovskite photovoltaics: Challenges, open questions, and opportunities. *APL Materials* 8: 100901. https://doi.org/10.1063/5.0022271
129. Rühle S (2017) The detailed balance limit of perovskite/silicon and perovskite/CdTe tandem solar cells. *Phys Status Solidi A* 214: 1600955. https://doi.org/10.1002/pssa.201600955
130. Sheng R, Ho-Baillie AWY, Huang SJ, et al. (2015) Four-terminal tandem solar cells using $CH_3NH_3PbBr_3$ by spectrum splitting. *J Phys Chem Lett* 6: 3931−3934. https://doi.org/10.1021/acs.jpclett.5b01608

131. Sani F, Shafie S, Lim HN (2018) Advancement on lead-free organic-inorganic halide perovskite solar cells: A review. *Materials* 11: 1008. https://doi.org/10.3390/ma11061008
132. Righetto M, Caicedo-Dávila S, Sirtl MT, et al. (2023) Alloying effects on charge-carrier transport in silver–bismuth double perovskites. *J Phys Chem Lett* 14: 10340–10347 https://doi.org/10.1021/acs.jpclett.3c02750
133. Bartesaghi D, Slavney AH, Gélvez-Rueda MC, et al. (2018) Charge carrier dynamics in $Cs_2AgBiBr_6$ double perovskite. *J Phys Chem C* 122: 4809–4816. https://doi.org/10.1021/acs.jpcc.8b00572
134. Joshua-Leveillee GV, Giustino F (2021) Phonon-limited mobility and electronphonon coupling in lead-free halide double perovskites. *J Phys Chem Lett* 12: 4474–4482. https://doi.org/10.1021/acs.jpclett.1c00841
135. Lin H, Zhou C, Tian Y (2018) Low-dimensional organometal halide perovskites. *ACS Energy Lett* 3: 54−62. https://doi.org/10.1021/acsenergylett.7b00926
136. Han D, Shi H, Ming W, et al. (2018) Unraveling luminescence mechanisms in zero-dimensional halide perovskites. *J Mater Chem C* 6: 6398−6405. https://doi.org/10.1039/C8TC01291A
137. Duan D, Ge C, Rahaman MZ, et al. (2023) Recent progress with one-dimensional metal halide perovskites: from rational synthesis to optoelectronic applications. *NPG Asia Mater* 15: 8. https://doi.org/10.1038/s41427-023-00465-0
138. Qiu T, Hu Y, Xu F (2018) Recent advances in one-dimensional halide perovskites for optoelectronic applications. *Nanoscale* 10: 20963−20989. https://doi.org/10.1039/C8NR05862H
139. Chen X, Zhou H, Wang H (2021) 2D/3D halide perovskites for optoelectronic devices. *Front Chem* 9. https://doi.org/10.3389/fchem.2021.715157
140. Fiorentino F, Albaqami MD, Poli I, et al. (2022) Thermal- and light-induced evolution of the 2D/3D interface in lead-halide perovskite films. *ACS Appl Mater Interfaces* 14: 34180−34188. https://doi.org/10.1021/acsami.1c09695
141. Kim EB, Akhtar MS, Shin HS, et al. (2021) A review on two-dimensional (2D) and 2D-3D multidimensional perovskite solar cells: Perovskites structures, stability, and photovoltaic performances. *J Photochem Photobiol C* 48: 100405. https://doi.org/10.1016/j.jphotochemrev.2021.100405
142. Etgar L (2018) The merit of perovskite's dimensionality; can this replace the 3D halide perovskite? *Energy Environ Sci* 11: 234−242. https://doi.org/10.1039/C7EE03397D
143. Marongiu D, Saba M, Quochi F (2019) The role of excitons in 3D and 2D lead halide perovskites. *J Mater Chem C* 7: 12006−12018. https://doi.org/10.1039/C9TC04292J
144. Moral RF, Perini CAR, Kodalle T, et al. (2024) Anion and cation migration at 2D/3D halide perovskite interfaces. *ACS Energy Lett* 9: 2703−2716. https://doi.org/10.1021/acsenergylett.4c00728
145. Filip MR, Hillman S, Haghighirad AA, et al. (2016) Band gaps of the lead-free halide double perovskites: $Cs_2BiAgCl_6$ and $Cs_2BiAgBr_6$ from theory and experiment. *J Phys Chem Lett* 7: 2579−2585. https://doi.org/10.1021/acs.jpclett.6b01041
146. McClure ETB, Windl MR, Woodward PMW (2016) Cs_2AgBiX_6 (X = Br, Cl): New visible light absorbing, lead-free halide perovskite semiconductors. *Chem Mater* 28: 1348−1354. https://doi.org/10.1021/acs.chemmater.5b04231

147. Luo SLJ, Wu H, Zhou Y, et al. (2018) $Cs_2AgInCl_6$ double perovskite single crystals: Parity forbidden transitions and their application for sensitive and fast UV photodetectors. *ACS Photonics* 5: 398. https://doi.org/10.1021/acsphotonics.7b00837
148. Zhou HC, Li Q, Luo G, et al. (2014) Interface engineering of highly efficient perovskite solar cells. *Science* 345: 542−546. https://doi.org/10.1126/science.1254050
149. De Quilettes DWV, Stranks SM, Nagaoka SD, et al. (2015) Impact of microstructure on local carrier lifetime in perovskite solar cells. *Science* 348: 683−686. https://doi.org/10.1126/science.aaa5333
150. Rui SHH, Chen T, Gui R, et al. (2023) Extracting energetic disorder in organic solar cells using percolation models. *ChemPhysMater* 2: 52–57. https://doi.org/10.1016/j.chphma.2022.03.002
151. Wang DD, Li YS, Yang YG, et al. (2024) Energetic disorder dominates optical properties and recombination dynamics in tin-lead perovskite nanocrystals. *eScience* 100279. https://doi.org/10.1016/j.esci.2024.100279
152. Yang C, Ma L, Xu Y (2022) Reduced energetic disorder enables over 14% efficiency in organic solar cells based on completely non-fused-ring donors and acceptors. *Sci China Chem* 65: 2604–2612. https://doi.org/10.1007/s11426-022-1449-4
153. Diez-Cabanes V, Samuele G, Beljonne D, et al. (2023) On the origin of energetic disorder in mixed halides lead perovskites. *Adv Optical Mater* 12: 2301105. https://doi.org/10.1002/adom.202301105
154. Liu Y, Banon JP, Frohna K, et al. (2023) The electronic disorder landscape of mixed halide perovskites. *ACS Energy Lett* 8: 250−258. https://doi.org/10.1021/acsenergylett.2c02352
155. Yin A, Zhang D, Cheung SH, et al. (2018) On the understanding of energetic disorder, charge recombination and voltage losses in all-polymer solar cells. *J Mater Chem C* 6: 7855–7863. https://doi.org/10.1039/C8TC02689K
156. Igbari F, Wang R, Wang ZK, et al. (2019) Composition stoichiometry of $Cs_2AgBiBr_6$ films for highly efficient lead-free perovskite solar cells. *Nano Lett* 19: 2066–2073. https://doi.org/10.1021/acs.nanolett.9b00238
157. Bush KA, Frohna K, Prasanna R, et al. (2018) Compositional engineering for efficient wide band gap perovskites with improved stability to photoinduced phase segregation. *ACS Energy Lett* 3: 428–435. https://doi.org/10.1021/acsenergylett.7b01255
158. Yang J, Zhang P, Wei SH (2018) Band structure engineering of $Cs_2AgBiBr_6$ perovskite through order–disordered transition: A first-principle study. *J Phys Chem Lett* 9: 31–35. https://doi.org/10.1021/acs.jpclett.7b02992
159. Kim J, Kim H, Mahesh C, et al. (2018) Impacts of cation ordering on bandgap dispersion of double perovskites. *APL Materials* 6: 084903. https://doi.org/10.1063/1.5027230
160. Liu Z, Li H, Qin C, et al. (2019) Solution-processed inorganic perovskite flexible photodetectors with high performance. *Nanoscale Res Lett* 14: 284. https://doi.org/10.1186/s11671-019-3120-x
161. Chilvery A, Das S, Guggilla P, et al. (2016) A perspective on the recent progress in solution-processed methods for highly efficient perovskite solar cells. *STAM* 17: 650–658. http://dx.doi.org/10.1080/14686996.2016.1226120
162. Seo JW, Noh JH, Seok SI (2016) Rational strategies for efficient perovskite solar cells. *Acc Chem Res* 49: 562–572. https://doi.org/10.1021/acs.accounts.5b00444

163. Arain Z, Liu C, Yang Y, et al. (2019) Elucidating the dynamics of solvent engineering for perovskite solar cells. *Sci China Mater* 62: 161–172. https://doi.org/10.1007/s40843-018-9336-1
164. Li J, Yang R, Que L, et al. (2019) Optimization of anti-solvent engineering toward high performance perovskite solar cells. *J Mater Res* 34: 2416–2424. https://doi.org/10.1557/jmr.2019.122
165. Duan J, Xu H, Sha W, et al. (2019) Inorganic perovskite solar cells: An emerging member of the photovoltaic community. *J Mater Chem A* 7: 21036–21068. https://doi.org/10.1039/C9TA06674H.
166. Li B, Fu L, Li S, et al. (2019) Pathways toward high-performance inorganic perovskite solar cells: Challenges and strategies. *J Mater Chem A* 7: 20494–20518. https://doi.org/10.1039/C9TA04114A
167. Wang P, Zhang X, Zhou Y, et al. (2018) Solvent-controlled growth of inorganic perovskite films in dry environment for efficient and stable solar cells. *Nat Commun* 9: 2225. https://doi.org/10.1038/s41467-018-04636-4
168. DeHoff RT (1999) Engineering of microstructures. *Mater Res* 2: 111–126. http://dx.doi.org/10.1590/S1516-14391999000300002
169. Clemens H, Mayer S, Scheu C (2017) Microstructure and properties of engineering materials: From fundamentals to applications, In: Staron P, Schreyer A, Clemens H, Mayer S, *In Neutrons and Synchrotron Radiation in Engineering Materials Science*, New York: John Wiley & Sons. https://doi.org/10.1002/9783527684489.ch1
170. Szuromi P (1997) Microstructural engineering of materials. *Science* 277: 1183. https://doi.org/10.1126/science.277.5330.1183
171. Chen L, Paillard C, Zhao HJ, et al. (2018) Tailoring properties of hybrid perovskites by domain-width engineering with charged walls. *npj Computat Mater* 4: 75. https://doi.org/10.1038/s41524-018-0134-3
172. Schade L, Wright AD, Johnson RD, et al. (2019) Structural and optical properties of $Cs_2AgBiBr_6$ double perovskite. *ACS Energy Lett* 4: 299–305. https://doi.org/10.1021/acsenergylett.8b02090
173. Lozhkina OA, Murashkina AA, Elizarov MS, et al. (2018) Microstructural analysis and optical properties of the halide double perovskite $Cs_2BiAgBr_6$ single crystals. *Chem Phys Lett* 694: 18–22. https://doi.org/10.1016/j.cplett.2018.01.031
174. Liu W, Liu Y, Wang J, et al. (2018) Twin domains in organometallic halide perovskite thin-films. *Crystals* 8: 216. https://doi.org/10.3390/cryst8050216
175. Liu S, Zheng F, Koocher NZ, et al. (2015) Ferroelectric domain wall induced band gap reduction and charge separation in organometal halide perovskites. *J Phys Chem Lett* 6: 693−699. https://doi.org/10.1021/jz502666j
176. You L, Zheng F, Fang L, et al. (2018) Enhancing ferroelectric photovoltaic effect by polar order engineering. *Sci Adv* 4: eaat3438. https://doi.org/10.1126/sciadv.aat3438
177. Li Y, Fu J, Mao X, et al. (2021) Enhanced bulk photovoltaic effect in two-dimensional ferroelectric $CuInP_2S_6$. *Nat Commun* 12: 5896. https://doi.org/10.1038/s41467-021-26200-3
178. Shockley W, Queisser HJ (1961) Detailed balance limit of efficiency of P-N junction solar cells. *J Appl Phys* 32: 510–511. https://doi.org/10.1063/1.1736034

179. Ihtisham ULH, Khan MI, Ullah A, et al. (2024) Bandgap reduction and efficiency enhancement in $Cs_2AgBiBr_6$ double perovskite solar cells through gallium substitution. *RSC Adv* 14: 5440–5448. https://doi.org/10.1039/D3RA08965G
180. Du KZ, Meng W, Wang X, et al. (2017) Bandgap engineering of lead-free double perovskite $Cs_2AgBiBr_6$ through trivalent metal alloying. *Angew Chem Int Ed* 8158–8162. https://doi.org/10.1002/anie.201703970
181. Yan K, Long M, Zhang T, et al. (2015) Hybrid halide perovskite solar cell precursors: Colloidal chemistry and coordination engineering behind device processing for high efficiency. *J Am Chem Soc* 137: 4460–4468. https://doi.org/10.1021/jacs.5b00321
182. Bellakhdar T, Nabi Z, Bouabdallah B, et al. (2022) Ab initio study of structural, electronic, mechanical and optical properties of the tetragonal $Cs_2AgBiBr_6$ halide double perovskite. *Appl Phys A* 128: 155. https://doi.org/10.1007/s00339-022-05276-8
183. Merabet B, Alamri H, Djermouni M (2012) Optimal bandgap of double perovskite la-substituted Bi_2FeCrO_6 for solar cells: An ab initio GGA+U study. *Chin Phys Lett* 34: 016101. https://doi.org/10.1088/0256-307X/34/1/016101
184. Alotaibi NH, Mustafa GM, Kattan NA (2022) DFT study of double perovskites Cs_2AgBiX_6 (X = Cl, Br): An alternative of hybrid perovskites. *J Solid State Chem* 313: 123353. https://doi.org/10.1016/j.jssc.2022.123353
185. Creutz SE, Crites EN, De-Siena MC, et al. (2018) Colloidal nanocrystals of lead-free double-perovskite (elpasolite) semiconductors: Synthesis and anion exchange to access new materials. *Nano Lett* 18: 1118–1123. https://doi.org/10.1021/acs.nanolett.7b04659
186. Hou P, Yang W, Wan N, et al. (2021) Precursor engineering for high-quality $Cs_2AgBiBr_6$ films toward efficient lead-free double perovskite solar cells. *J Mater Chem C* 9: 9659–9669. https://doi.org/10.1039/D1TC01786A
187. Kangsabanik J, Sugathan V, Yadav A, et al. (2018) Double perovskites overtaking the single perovskites: A set of new solar harvesting materials with much higher stability and efficiency. *Phys Rev Mater* 2: 055401. https://doi.org/10.1103/PhysRevMaterials.2.055401
188. Laporte O (1924) Die struktur des eisenspektrums. *Z Physik* 23: 135–175. https://doi.org/10.1007/BF01327582
189. Nathan R, Wolf BAC, Slavney AH, et al. (2021) Doubling the stakes: The promise of halide double perovskites. *Angew Chem Int Ed* 60: 2–17. https://doi.org/10.1002/anie.202016185
190. Fridkin VM (2001) Bulk photovoltaic effect in noncentrosymmetric crystals. *Crystallogr Rep* 46: 654–658. https://doi.org/10.1134/1.1387133
191. Gao P, Liu HJ, Huang YL (2016) Atomic mechanism of polarization-controlled surface reconstruction in ferroelectric thin films. *Nat Commun* 7: 11318. https://doi.org/10.1038/ncomms11318
192. Von Baltz WKR (1981) Theory of the bulk photovoltaic effect in pure crystals. *Phys Rev B* 23: 5590–5596. https://doi.org/10.1103/PhysRevB.23.5590
193. Young SM, Rappe AM (2012) First principles calculation of the shift current photovoltaic effect in ferroelectrics. *Phys Rev Lett* 109: 116601. https://doi.org/10.1103/PhysRevLett.109.116601

194. Young SM, Zheng F, Rappe AM (2012) First-principles calculation of the bulk photovoltaic effect in bismuth ferrite. *Phys Rev Lett* 109: 236601. https://doi.org/10.1103/PhysRevLett.109.236601
195. Harikesh PC, Wu B, Ghosh B, et al. (2018) Doping and switchable photovoltaic effect in lead-free perovskites enabled by metal cation transmutation. *Adv Mater* 30: 1802080. https://doi.org/10.1002/adma.201802080.
196. Lee D, Baek SH, Kim TH, et al. (2011) Polarity control of carrier injection at ferroelectric/metal interfaces for electrically switchable diode and photovoltaic effects. *Phys Rev B* 84: 125305. https://doi.org/10.1103/PhysRevB.84.125305
197. Li H, Li F, Shena Z, et al. (2021) Photoferroelectric perovskite solar cells: Principles, advances and insights. *Nano Today* 37: 101062. https://doi.org/10.1016/j.nantod.2020.101062
198. Tsien RY (2009) Constructing and exploiting the fluorescent protein paintbox (nobel lecture). *Chem Int Ed* 48: 5612–5626. https://doi.org/10.1002/anie.200901916
199. Liu HY, Zhang HY, Chen XG, et al. (2020) Molecular design principles for ferroelectrics: Ferroelectrochemistry. *J Am Chem Soc* 142: 15205−15218. https://dx.doi.org/10.1021/jacs.0c07055
200. Shi PP, Tang YY, Li PF, et al. (2016) Symmetry breaking in molecular ferroelectrics. *Chem Soc Rev* 45: 3811−3827. https://doi.org/10.1039/C5CS00308C
201. Li K, Li ZG, Lu J, et al. (2022) Origin of ferroelectricity in two prototypical hybrid organic-inorganic perovskites. *J Am Chem Soc* 144: 816–823. https://doi.org/10.1021/jacs.1c10188
202. Anderson PW, Blount EI (1965) Symmetry considerations on martensitic transformations: 'Ferroelectric' metals? *Phys Rev Lett* 14: 217–219. https://doi.org/10.1103/PhysRevLett.14.217
203. Shi Y, Guo Y, Wang X, et al. (2013) A ferroelectric-like structural transition in a metal. *Nat Mater* 12: 1024–1027. https://doi.org/10.1038/NMAT3754
204. Yildirim T (2013) Ferroelectric soft phonons, charge density wave instability, and strong electron-phonon coupling in BiS_2 layered superconductors: A first-principles study. *Phys Rev B* 87: 020506(R). https://doi.org/10.48550/arXiv.1210.2418
205. Rakita Y, Bar-Elli O, Meirzadeha E, et al. (2017) Tetragonal $CH_3NH_3PbI_3$ is ferroelectric. *PNAS* 114: E5504–E5512. https://doi.org/10.1073/pnas.1702429114
206. Alexe M, Hasse D (2011) Tip-enhanced photovoltaic effects in bismuth ferrite. *Nat Commun* 2: 256. https://doi.org/10.1038/ncomms1261
207. Liao WQ, Zhang Y, Hu CL (2015) A lead-halide perovskite molecular ferroelectric semiconductor. *Nat Commun* 6: 7338. https://doi.org/10.1038/ncomms8338
208. Guyonnet J (2014) Domain walls in ferroelectric materials, In: Guyonnet J, *Ferroelectric Domain Walls*, Cham: Springer, 7–24. https://doi.org/10.1007/978-3-319-05750-7_2
209. Rakita Y (2016) $CH_3NH_3PbBr_3$ is not pyroelectric, excluding ferroelectricenhanced photovoltaic performance. *APL Mater* 4: 051101. http://dx.doi.org/10.1063/1.4949760
210. Landau L, Lifshitz E (1935) On the theory of the dispersion of magnetic permeability in ferromagnetic bodies. *Phys Z Sowjetunion* 8: 101–114. https://doi.org/10.1016/B978-0-08-036364-6.50008-9

211. Kittel C (1946) Theory of the structure of ferromagnetic domains in films and small particles. *Phys Rev* 70: 965–971. https://doi.org/10.1103/PhysRev.70.965
212. Guyonnet J (2014) *Ferroelectric Domain Walls*, Cham: Springer. https://link.springer.com/book/10.1007/978-3-319-05750-7
213. Sherkar TS, Anton KLJ (2016) Can ferroelectric polarization explain the high performance of hybrid halide perovskite solar cells? *Phys Chem Chem Phys* 18**:** 331–338. https://doi.org/10.1039/C5CP07117H
214. Nye JF (1985) *Physical Properties of Crystals*, Oxford: Oxford University Press.
215. Lines ME, Glass AM (1979) *Principles and Applications of Ferroelectrics and Related Materials*, Oxford: Oxford University Press. https://doi.org/10.1093/acprof:oso/9780198507789.001.0001
216. Mitsui T, Tatsuzaki I, Nakamura E (1976) *An Introduction to the Physics of Ferroelectrics*, London: Gordon and Breach.
217. Jaffe BC, Jaffe HW (1971) *Piezoelectric Ceramics*, New York: Academic Press, 313–338. https://doi.org/10.1016/B978-0-323-89952-9.00005-1
218. Ballato A (1995) Piezoelectricity: Old effect, new thrusts. *IEEE T Ultrason Ferr* 42: 916–926. https://doi.org/10.1109/58.464826
219. Park H, Ha C, Lee JH (2020) Advances in piezoelectric halide perovskites for energy harvesting applications. *J Mater Chem A* 8: 24353–24367. https://doi.org/10.1039/d0ta08780g
220. Rashkeev S, El-Mellouhi F, Kais S, et al. (2015) Domain walls conductivity in hybrid organometallic perovskites and their essential role in $CH_3NH_3PbI_3$ solar cell high performance. *Sci Rep* 5: 11467. https://doi.org/10.1038/srep11467
221. Ma J, Wang LW (2015) Nanoscale charge localization induced by random ori-entations of organic molecules in hybrid perovskite $CH_3NH_3PbI_3$. *Nano Lett* 15: 248–253. https://doi.org/10.1021/nl503494y
222. Liu S, Zheng F, Grinberg I, et al. (2016) Photoferroelectric and photopiezoelectric properties of organometal halide perovskites. *J Phys Chem Lett* 7: 1460–1465. https://doi.org/10.1021/acs.jpclett.6b00527
223. Damjanovic D (1998) Ferroelectric, dielectric and piezoelectric properties of ferroelectric thin films and ceramics. *Rep Prog Phys* 61: 1267. https://doi.org/10.1088/0034-4885/61/9/002
224. Sahoo A, Paul T, Makani NH, et al. (2022) High piezoresponse in low-dimensional inorganic halide perovskite for mechanical energy harvesting. *Sustain Energ Fuels* 6: 4484–4497. https://doi.org/10.1039/d2se00786j
225. Butler KT, Frost JM, Walsh A (2015) Ferroelectric materials for solar energy conversion: Photoferroics revisited. *Energy Environ Sci* 8: 838–848. https://doi.org/10.1039/C4EE03523B
226. Chelil N, Sahnoun M, Benhalima Z, et al. (2023) Insights into the relationship between ferroelectric and photovoltaic properties in $CsGeI_3$ for solar energy conversion. *RSC Adv* 13: 1955–1963. https://doi.org/10.1039/D2RA06860E
227. Zhang Y, Liu Y, Wang ZL (2011) Fundamental theory of piezotronics. *Adv Mater* 23: 3004–3013. https://doi.org/10.1002/adma.201100906

228. Hu Y, Chang Y, Fei P, et al. (2010) Designing the electric transport characteristics of zno micro/nanowire devices by coupling piezoelectric and photoexcitation effects. *ACS Nano* 4: 1234–1240. https://doi.org/10.1021/nn901805g
229. Hu Y, Zhang Y, Chang Y, et al. (2010) Optimizing the power output of a ZnO photocell by piezopotential. *ACS Nano* 4: 4220–4224. https://doi.org/10.1021/nn1010045
230. He JH, Liu J, Chen LJ, et al (2007) Piezoelectric gated diode of a single ZnO nanowire. *Adv Mater* 19: 781. https://doi.org/10.1002/adma.200602918
231. Wang X, Zhou J, Song J, et al. (2006) Piezoelectric field effect transistor and nanoforce sensor based on a single ZnO nanowire. *Nano Lett* 6: 2768. https://doi.org/10.1021/nl061802g
232. Lao CS, Kaung Q, Wang ZL, et al (2007) Polymer functionalized piezoelectric-FET as humidity/chemical nanosensors. *Appl Phys Lett* 90: 262107. https://doi.org/10.1063/1.2748097
233. Wang ZL, Song J (2006) Piezoelectric nanogenerators based on zinc oxide nanowire arrays. *Science* 312: 242. https://doi.org/10.1126/science.112400
234. Wang X, Song J, Liu J, et al. (2007) Direct-current nanogenerator driven by ultrasonic waves. *Science* 316: 102. https://doi.org/10.1126/science.1139366
235. Qin Y, Wang X, Wang ZL (2008). Microfibre-nanowire hybrid structure for energy scavenging. *Nature* 451: 809. https://doi.org/10.1038/ncomms13146
236. Weber ZD (1978) $CH_3NH_3PbX_3$ ein Pb(II)-system mit kubischer perowskitstruktur/$CH_3NH_3PbX_3$, a Pb(II)-system with cubic perovskite structure. *Naturforsch* 33: 1443. https://doi.org/10.1515/znb-1978-1214
237. Poglitsch DWA (1987) Dynamic disorder in methylammoniumtrihalogenoplumbates(II) observed by millimeter-wave spectroscopy. *J Chem Phys* 87: 6373. https://doi.org/10.1063/1.453467
238. Frost JM, Butler KT, Brivio F, et al. (2014) Atomistic origins of high-performance in hybrid halide perovskite solar cells. *Nano Lett* 14: 2584. https://doi.org/10.1021/nl500390f
239. Frost JM, Butler KT, Walsh A (2014) Molecular ferroelectric contributions to anomalous hysteresis in hybrid perovskite solar cells. *APL Mater* 2: 081506. https://doi.org/10.1063/1.4890246
240. Coll AGM, Marza EM, Almora O, et al. (2015) Polarization switching and light-enhanced piezoelectricity in lead halide perovskites. *J Phys Chem Lett* 6: 140 https://doi.org/10.1021/acs.jpclett.5b00502
241. Kim YJ, Dang TV, Choi HJ, et al. (2016) Piezoelectric properties of $CH_3NH_3PbI_3$ perovskite thin films and their applications in piezoelectric generators. *J Mater Chem A* 4: 756. https://doi.org/10.1039/C5TA09662F
242. Shahrokhi S, Gao W, Wang Y, et al. (2020) Emergence of ferroelectricity in halide perovskites. *Small Methods* 4: 2000149. https://doi.org/10.1002/smtd.202000149
243. Ding R, Liu H, Zhang X, et al. (2016) Flexible piezoelectric nanocomposite generators based on formamidinium lead halide perovskite nanoparticles. *Adv Funct Mater* 26: 7708. https://doi.org/10.1002/adfm.201602634
244. Mohandes A, Moradi M, Nadgaran H (2021) Numerical simulation of inorganic $Cs_2AgBiBr_6$ as a lead-free perovskite using device simulation SCAPS-1D. *Opt Quantum Electron* 53: 319. https://doi.org/10.1007/s11082-021-02959-z

245. Slavney AH, Leppert L, Bartesaghi D, et al. (2017) Defect-induced band-edge reconstruction of a bismuth-halide double perovskite for visible-light absorption. *J Am Chem Soc* 139: 5015–5018. https://doi.org/10.1021/jacs.7b01629
246. Wang F, Bai S, Tress W, et al. (2018) Defects engineering for high-performance perovskite solar cells. *npj Flex Electron* 2: 22. https://doi.org/10.1038/s41528-018-0035-z
247. Han TH, Tan S, Xue J, et al. (2019) Interface and defect engineering for metal halide perovskite optoelectronic devices. *Adv Mater* 31: e1803515. https://doi.org/10.1002/adma.201803515
248. Xu J, Liu JB, Liu BX, et al. (2019) Defect engineering of grain boundaries in lead-free halide double perovskites for better optoelectronic performance. *Adv Funct Mater* 29: 1805870. https://doi.org/10.1002/adfm.201805870
249. Ramesha R (2018) Defect engineering using crystal symmetry. *PNAS* 115: 9344–9346 https://doi.org/10.1073/pnas.1812554115
250. Samanta M, Ahmed SI, Chattopadhyay KK, et al. (2020) Role of various transport layer and electrode materials in enhancing performance of stable environment-friendly Cs_2TiBr_6 solar cell. *Optik* 217: 164805. https://doi.org/10.1016/j.ijleo.2020.164805
251. He Y, Xu L, Zheng H, et al. (2021) Numerical exploration of lead-free inorganic perovskite Cs_2TiBr_6 solar cell. *J Phys Conf Ser* 2021: 012069. https://doi.org/10.1088/1742-6596/2021/1/012069
252. Jani MR, Islam MT, Al Amin SM, et al. (2020) Exploring solar cell performance of inorganic Cs_2TiBr_6 halide double perovskite: A numerical study. *Superlattices Microstruct* 146: 106652. https://doi.org/10.1016/j.spmi.2020.106652
253. Sultana F, Jannat F, Ahmed S, et al. (2023) A comparative numerical approach between lead-free inorganic Cs_2TiBr_6 and Cs_2PtI_6-based perovskite solar cells. *Results in Opt* 13: 100567. https://doi.org/10.1016/j.rio.2023.100567
254. He Y, Zheng H, Huang S, et.al. (2021) Defect investigation of Ti-based vacancy-ordered double perovskite solar cell using SCAPS-1D. *J Phys Conf Ser* 2044: 012100. https://doi.org/10.1088/1742-6596/2044/1/012100
255. Hussain I, Tran HP, Jaksik J, et al. (2018) Functional materials, device architecture, and flexibility of perovskite solar cell. *Emergent Mater* 1: 133–154. https://doi.org/10.1007/s42247-018-0013-1
256. Kopacic I, Friesenbichler B, Hoefler S, et al. (2018) Enhanced performance of germanium halide perovskite solar cells through compositional engineering. *ACS Appl Energy Mater* 1: 343–347. https://doi.org/10.1021/acsaem.8b00007
257. Song Z, Watthage SC, Phillips AB, et al. (2016) Pathways toward high-performance perovskite solar cells: Review of recent advances in organo-metal halide perovskites for photovoltaic applications. *JPE* 6: 022001. https://doi.org/10.1117/1.JPE.6.022001
258. Tran TT, Pennella JR, Chamorro JR, et al. (2017) Designing indirect–direct bandgap transitions in double perovskites. *Mater Horiz* 4: 688. https://doi.org/10.1039/C7MH00239D
259. Giustino F, Snaith HJ (2016) Toward lead-free perovskite solar cells. *ACS Energy Lett* 1: 1233. https://doi.org/10.1021/acsenergylett.6b00499
260. Sun Q, Wang J, Yin JW, et al. (2018) Bandgap engineering of stable lead-free oxide double perovskites for photovoltaics. *Adv Mater* 30: 1705901. https://doi.org/10.1002/adma.201705901

261. Du KZ, Wang X, Han Q, et al. (2017) Heterovalent B-site Co-alloying approach for halide perovskite bandgap engineering. *ACS Energy Lett* 2: 2486. https://doi.org/10.1021/acsenergylett.7b00824